Version of Record: https://www.sciencedirect.com/science/article/pii/S0168192315001458
Manuscript_6bb98c75191fbde9dce561c06e09b047

Empirical Estimation of Daytime Net Radiation from Shortwave Radiation and Ancillary Information

Bo Jiang[1], Yi Zhang[2], Shunlin Liang[1, 2], Georg Wohlfahrt[3], Altaf Arain[4], Alessandro Cescatti[5], Teodoro Georgiadis[6], Kun Jia[1], Gerard Kiely[7], Magnus Lund[8], Leonardo Montagnani[9], Vincenzo Magliulo[10], Penelope Serrano Ortiz[11], Walter Oechel[12], Francesco Primo Vaccari[13], Yunjun Yao[1], Xiaotong Zhang[1]

1. State Key Laboratory of Remote Sensing Science, and School of Geography, Beijing Normal University, Beijing 100875, China; 2. Department of Geographical Sciences, University of Maryland, College Park, MD 20742, USA; 3. Institute of Ecology, University of Innsbruck, Innsbruck, Austria; 4. School of Geography and Earth Sciences and McMaster Centre for Climate Change, McMaster University, Hamilton, Ontario, CanadaL8S4K1; 5. European Commission, Joint Research Center, Institute for Environment and Sustainability, Ispra, Italy; 6. CNR-Institute of Biometeorology, via Gobetti 101, 40129 Bologna, Italy; 7. Civil and Environmental Engineering, and Environmental Research Institute, University College Cork, Ireland; 8. Arctic Research Centre, Department of Bioscience, Aarhus University, Frederiksborgvej 399, DK-4000 Roskilde, Denmark; 9. Faculty of Science and Technology, Free University of Bolzano, Piazza Università 5, 39100 Bolzano, Italy; 10. CNR-ISAFOM, Institute for Mediterranean Agricultural and Forest Systems, National Research Council, via Patacca 85, 80040 Ercolano (Napoli), Italy; 11. Dpto. Ecología, Facultad de Ciencias, Universidad de Granada; 12.Global Change Research Group, San Diego State University, San Diego, CA 92182, USA; 13.IBIMET-CNR Institute of Biometeorology National Research Council, via G. Caproni 8, 50145 Firenze, Italy

Corresponding author: Bo Jiang (bojiang@bnu.edu.cn)

Abstract

All-wave net surface radiation is greatly needed in various scientific research and applications. Satellite data have been used to estimate incident shortwave radiation, but hardly to estimate all-wave net radiation due to the inference of clouds on longwave radiation. A practical solution is to estimate all-wave net radiation empirically from shortwave radiation and other ancillary information. Since existing models were developed using a limited number of ground observations, a comprehensive evaluation of these models using a global network of representative measurements is urgently required. In this study, we developed a new day-time net radiation estimation model and evaluated it against seven commonly used existing models using radiation measurements obtained from 326 sites around the world from 1991–2010. MERRA re-analysis products from which the meteorological data were derived and remotely sensed products during the same period were also used. Model evaluations were performed in both global mode (all data were used to fit the models) and conditional mode (the data were divided into four subsets based on the surface albedo and vegetation index, and the models were fitted separately). Besides, the factors (i.e. albedo, air temperature, and NDVI) that may impact the estimation of all-wave net radiation were also extensively explored. Based on these evaluations, the fitting RMSE of the new developed model was approximately 40.0 Wm^{-2} in the global mode and varied between 18.2 and 54.0 Wm^{-2} in the conditional mode. We found that it is better to use net shortwave radiation (including surface albedo) than the incident shortwave radiation nearly in all models. Overall, the new model performed better than other existing linear models.

Keywords: Net radiation, Shortwave radiation, Empirical model, Remotely sensed product

1. Introduction

All-wave net surface radiation (R_n) constitutes the available radiative energy at the surface, and as such regulates most biological and physical processes, such as evapotranspiration (Lu et al., 2014; Lu et al., 2013; Wang and Liang, 2008), photosynthesis and turbulent and conductive heat fluxes. Thus, accurate estimates of R_n are essential for understanding the land surface energy distribution, the formation and transformation of air masses, snow melting calculations(Male and Granger, 1981), modeling crop growth, and addressing water resource management (Bisht and Bras, 2011; Hwang et al., 2012). Estimation of R_n is necessary because it is a key input for land surface process models, and are also used routinely to calculate evapotranspiration(Monteith, 1965), which is a critical component of agricultural, hydrological, and ecological research.

R_n is the difference between the incoming and outgoing shortwave and longwave radiation fluxes at the surface. Mathematically described as:

$$\begin{aligned} R_n &= R_{ns} + R_{nl} \\ R_{ns} &= R_{si} - R_{so} = (1-\alpha)R_{si} \\ R_{nl} &= R_{li} - R_{lo} \end{aligned} \tag{1}$$

Where R_{si} is the incoming shortwave radiation (Wm^{-2}), R_{so} is the reflected outgoing shortwave radiation (Wm^{-2}), which is calculated by $R_{so}=\alpha*R_{si}$, α is the shortwave broadband albedo (dimensionless), thus R_{ns} is the net shortwave radiation, R_{li} is the incoming longwave radiation (Wm^{-2}), R_{lo} is the outgoing longwave radiation (Wm^{-2}), and R_{nl} is the net longwave radiation (Wm^{-2}). R_n is normally positive during the daytime because net shortwave radiation dominates, but negative during the nighttime because net longwave radiation dominates (Allen et al., 1998).

If all four components of Eq. (1) are known, the calculation of R_n is straightforward. Indeed, many radiation measurement towers measure these four components of radiation, thereby allowing us to determine R_n at individual points. Various satellite observations have been used to generate radiation products at regional and global scales (Liang et al., 2010; Liang et al., 2013b; Tang and Li, 2008; Tang et al., 2006; Wang and Liang, 2009b; Zhang et al., 2014). Satellite observations from the visible to near-infrared spectrum have been used for estimating incident solar radiation and surface albedo, and thermal-infrared data for estimating longwave radiation. There are roughly two types of algorithms for estimating radiation(Liang et al., 2010), one calculates radiative quantities from the derived satellite products of all relevant atmospheric and surface variables (e.g., aerosol, cloud, atmospheric temperature profile), and another estimates radiation directly from satellite observed radiance using a regression equation established from extensive radiative transfer simulations.

However, frequent cloud coverage implies that it is extremely difficult to estimate R_n

directly from satellite data, particularly longwave radiation component, because clouds block the surface information from reaching the sensors. Since incident shortwave radiation dominates day-time net radiation, methods have been developed to estimate the incident shortwave radiation from satellite data (Liang et al., 2010). Satellite data include information from both atmosphere and surface. From the "clearest" observations (less atmospheric signals) during a temporal window, surface reflectance/albedo can be retrieved, which can be assumed invariant during a short period of time. As long as surface information is known, we can determine the remaining atmospheric component that leads to estimation of incident shortwave radiation (Liang et al., 2006). One of the challenges is the need for multiple observations during a day for estimating day-time radiation but most polar-orbiting satellite sensors, such as MODIS, observe the same surface only a couple of times daily. One solution is to combine both polar-orbiting satellite data with geostationary satellite(Zhang et al., 2014), for example, the Global Land Surface Satellite (GLASS) radiation products at 5km spatial resolution and 3-hour temporal resolution(Liang et al., 2013a; Liang et al., 2013c). Thus, an important research goal presently is to develop robust methods for the empirical estimation of R_n from incident shortwave radiation.

Although important information can be derived from sustained and uninterrupted measurements of R_n over a surface, R_n measurements are only available from a small number of representative radiometric observatories because expensive instruments and constant maintenance are required (Monteith and Unsworth, 1990). To overcome the lack of experimental observations, R_n needs therefore to be estimated from empirical relationships based on physical considerations and meteorological data. From a practical view point, it is important that R_n can be determined from relationships that are not location-dependent so they are more universally applicable and easy to use (Al-Riahi et al., 2003). Consequently, numerous attempts have been made to calculate R_n based on different empirical methods. Two main types of empirical methods can be classified according to previous studies. The first type of methods estimates R_n from incoming shortwave radiation R_{si} and other meteorological variables using simple linear regression (see Section 2.1.1). The second type of methods estimates R_n by calculating the individual components in Eq.(1) separately, where each component is estimated empirically or physically (Allen et al., 2011). The first type of methods is used more widely, while the second one often generates hybrid models with mixed empirical and physical sub-models.

Many of these empirical models were developed based on observational data from specific locations. Thus, evaluating their performance in various environmental conditions is a critical issue. Several studies have been conducted to evaluate the performance of various empirical R_n estimation methods. Iziomon et al. (2000) compared four types of regression models in three sites at different altitudes in the southern Upper Rhine valley between Germany and Switzerland, and defined a model as a "basic regression model" where R_n was only related to R_{si}. The limitations associated with basic regression models were identified and improvements were suggested such as incorporating a clearness index for characterizing the effects of clouds on both shortwave and longwave radiation and air temperature for better estimation of longwave radiation (see equations (4) and (6) below). Alados et al. (2003) also compared the basic regression model with a model that was modified by including albedo and seasonal information for a period of 38 months at a semi-arid region site in Southeastern Spain. They concluded that seasonal information yielded significant improvements for a semi-arid shrubland, but only slight improvements were obtained by incorporating albedo information. Kjaersgaard et al. (2007) tested six commonly used empirical models, including basic regression, multivariate regression, and hybrid models coupled to physical Stefan-Boltzmann relationships, at two independent temperate sites in Denmark for 32 and 7 years. Kjaersgaard et al. (2009) focused mainly on comparisons of three net longwave radiation parameterization models under two climate regimes in Denmark and Spain respectively. Kjaersgaard et al. (2007) showed that various regression models that rely on the local calibration of model coefficients should be derived from a time series that comprises at least 5 years of data, and they also showed that physically-based models are more suitable. They concluded that the performance of these models is generally best in the summertime and worst in the wintertime. Better performance in the summertime and worse performance in the wintertime for various radiation parameterization schemes, both the physical and empirical, are due to the higher signal-to-noise ratio (STNR) for higher magnitudes of radiation in the summertime but lower STNR for lower magnitudes of radiation in the wintertime. Similarly, Sentelhas and Gillespie(2008) evaluated four types of models to estimate the hourly R_n at a grass site in mid-latitudes in Canada for a 58-day period during the growing season in 2003. These models were based on different combinations of R_{si}, meteorological variables (air temperature and relative humidity), and cloud cover information. The results showed that these models performed well and they were generally able to obtain similar hourly R_n values as measured, but they performed better in clear sky conditions rather than overcast conditions, and the incorporation of cloud information did not seem to significantly improve these estimates of R_n. The reason for better performances of these models in clear sky conditions is exactly the same as in the summertime because of the higher STNR of the radiation measurements.

Most previous studies have evaluated empirical R_n estimation methods in different environmental conditions as described above, but they still have several limitations. The number of R_n validation sites used in early works was in fact typically less than five, which means that the land cover and climatic conditions encompassed were limited, so that the conclusions of these studies are not suitable to be adopted universally. Also, since long-term time series of radiation measurements are not easy to collect, most studies focused on a short-term period. Several studies have suggested that at least 5-year observations are needed for fitting empirical models (Kjaersgaard et al., 2007; Wang and Liang, 2009a). This may be one of the reasons why the performance of the same model varied greatly among studies. Another important limitation of these empirical approaches is that they do not accommodate terrain effects on incoming solar radiation. This simplification could result in significant errors over mountainous areas where aspect, slope, and elevation can greatly determine the globe incoming solar radiation and consequently net radiation for applications associated with ET estimation, ecosystem and climate modeling (Gao et al., 2008; Long et al., 2010; Wu et al., 2006). Finally, new empirical models that use shortwave radiation developed recently have not been evaluated and compared with other models.

The objective of this study is to identify the most robust empirical models for estimating daytime (defined as the time period between sunrise and sunset) R_n from incident and/or net shortwave radiation and other meteorological variables that are suitable to be used at global scale. The strategy to achieve this objective is to collect the most comprehensive and representative ground measurements data sets across the world to test all available empirical models. In this study, observed radiation data were obtained from 326 sites, and were collected around the world since the 1990s from 12 observing networks. Based on these evaluations, we propose a new empirical model for estimating the daytime R_n.

The remainder of this paper is organized as follows. The different models are introduced in Section 2. Section 2 also describes the site information, remotely sensed and re-analysis data, and the data processing procedure. The results of the analyses and discussions are presented in Section 3. A Summary is given in Sections4.

2. Methodology and data

2.1 Methodology

2.1.1Overview of the empirical models

We present seven types of empirical models and their common feature is that the R_n is estimated linearly from the incoming shortwave radiation.

Model 1 (*mod1*) is the simplest:

$$R_n = a_1 R_{si} + b_1 \tag{2}$$

where a_1 and b_1 are coefficients. The main advantage of *mod1* is its simplicity since its only requirement is the incoming shortwave radiation. However, *mod1* does not correct for the net longwave radiation or for the seasonal changes in surface albedo (Kjaersgaard et al., 2007 1213).

Model 2 (*mod2*) is very similar to *mod1* but it uses net shortwave radiation instead. The implicit inclusion of albedo was first introduced by Kaminsky and Dubayah(1997):

$$R_n = a_2 R_{ns} + b_2 = a_2 R_{si}(1-\alpha) + b_2 \tag{3}$$

where a_2 and b_2 are coefficients. The authors concluded that the use of net shortwave radiation can make the model almost independent of the cloud cover, time of day, or day of year.

To take into account the impacts of clouds, Iziomon et al. (2000) found that the inclusion of a clearness index ($CI = {R_{si}}/{R_{se}}$) can improve the daytime R_n estimation:

$$R_n = a_3 R_{si} + b_3 CI + c_3 \tag{4}$$

where a_3, b_3, and c_3 are coefficients, CI is the clearness index (dimensionless), and R_{se} is the extra-terrestrial irradiance, which is calculated as follows(Irmak et al., 2003):

$$\begin{aligned} R_{se} &= \frac{1440 G_{sc} dr}{\pi}[\omega_s \sin(\phi)\sin(\delta) + \cos(\phi)\cos(\delta)\sin(\omega_s)] \\ d_r &= 1 + 0.033\cos(\frac{2\pi DOY}{365}) \\ \delta &= 0.409\sin(\frac{2\pi DOY}{365} - 1.39) \\ \omega_s &= \arccos[-\tan(\phi)\tan(\delta)] \end{aligned} \tag{5}$$

where G_{sc} is the solar constant (0.0820 $MJm^{-2} \cdot \min^{-1}$), d_r is the inverse relative distance from the Earth to the Sun, ω_s is the sunset hour angle (*rad*), φ is the latitude

(rad), δ is the solar declination (rad), and DOY is the day of the year. This model is defined as *mod3* in this study.

Iziomon et al. (2000) also found that surface air temperature affects the estimation of longwave radiation and eventually net radiation, and this model is defined as *mod4*:

$$R_n = a_4 R_{si}(1-\alpha) + b_4 \sigma T_{a,K}^4 + c_4 \tag{6}$$

where $T_{a,K}$ is the absolute air temperature, σ =Stefan-Boltzmann constant ($5.67 \times 10^{-8} WK^{-4} m^{-2}$), and a_4, b_4, and c_4 are coefficients. Surface air temperature determines downward longwave radiation of the atmosphere, and also is a proxy of surface skin temperature that largely determines surface upwelling longwave radiation, The authors found out that *mod4* performed better monthly than hourly.

Irmak et al. (2003) also linked R_n to a set of meteorological variables. However, Kjaersgaard et al. (2007) showed that some variables (i.e., the daily maximum and minimum air temperatures) are inter-correlated, which may cause multicollinearity and make the prediction model less stable. Therefore, the regression model proposed by Irmak et al.(2003) was modified by Kjaersgaard et al.(2007), and this model is defined as *mod5* as follows:

$$R_n = a_5 R_{si} + b_5 T_{a,°C} + c_5 d_r + d_5 \tag{7}$$

Where $T_{a,°C}$ is the mean air temperature (°C), d_r is the inverse relative Earth-Sun distance defined in Eq. (5), and a_5, b_5,, c_5, and d_5 are coefficients. Kjaersgaard et al.(2007) concluded that *mod5* tended to overestimate R_n slightly in some seasons but it still performed better than the original model proposed by (Irmak et al., 2003).

Holtslag and Van Ulden(1983) proposed a relationship between the shortwave net radiation, surface air temperature and cloud cover:

$$R_n = \frac{R_{si}(1-\alpha) + D_1 T_{a,K}^6 - \sigma T_{a,K}^4 + D_2 N}{1 + D_3} \quad (8)$$

where D_1= $5.31 \times 10^{-13} Wm^{-2} \cdot K^{-6}$ is an empirical constant suggested by Swinbank(1963), N is the total cloud cover fraction, $T_{a,K}$ is mean daily absolute air temperature (K), D_2 and D_3 are also empirical constants, and D_3 denotes the heating coefficient for the surface. The authors treated the term $D_1 T_{a,K}^6$ as the theoretical incoming longwave radiation and $\sigma T_{a,K}^4$ as the theoretical outgoing longwave radiation. Thus, $R_{si}(1-\alpha) + D_1 T_{a,K}^6 - \sigma T_{a,K}^4$ represents the theoretical net radiation, while all the other terms are used to correct the theoretical net radiation to the actual net radiation. Cloud data were not easy to collect, so we used $N = 1 - CI$ instead in the present study. D_2 and D_3 have been derived by Al-Riahi et al.(2003) using locally collected data. Therefore, we modified the original model as follows and defined it as *mod6*:

$$R_n = a_6[R_{si}(1-\alpha) + D_1 T_{a,K}^6 - \sigma T_{a,K}^4] + b_6 CI + c_7 \quad (9)$$

where a_6, b_6, and c_7 are coefficients. Al-Riahi et al.(2003) validated the original model (Eq. (8)) in an area of Baghdad that was covered by grass and found that the model performance was best under clear sky conditions (R^2> 0.99 in summer).

Although *mod6* incorporates the influence of clouds, the impact of the land surface is not considered. Learning from the study of Wang and Liang(2009a) (see also equation (11)), the normalized difference vegetation index (NDVI) could be a good indicator to represent the land surface in R_n estimation. Therefore, we improved *mod6* by incorporating the remotely sensed *NDVI* and relative humidity ($RH_{\%}$) after multiple trial experiments, and we denote this model as "*modnew*":

$$\begin{aligned} Rn = a_{new}[R_{si}(1-\alpha) + D_1 T_{a,K}^{6} - \sigma T_{a,K}^{4}] + b_{new} CI \\ + c_{new} NDVI + d_{new} RH_{\%} + e_{new} \end{aligned} \tag{10}$$

where a_{new}, b_{new}, c_{new}, d_{new}, and e_{new} are coefficients, and the other variables are the same as those used in *mod6*.

Wang and Liang (2009a) developed a multivariate linear regression model based on solar shortwave radiation and conventional meteorological observations and satellite retrievals (*NDVI* and albedo), as follows:

$$R_n = R_{si}(1-\alpha)(a + bT_{\min,°C} + cDT_{a,°C} + dNDVI + eRH_{\%}) \tag{11}$$

where $T_{min,℃}$ is the daily minimum air temperature and $DT_{a,°C}$ is the daily diurnal air temperature range. It was found that this model could readily generate a large bias, so a constant term was added in this study. To ensure consistency, this model (*mod7*) is expressed as follows:

$$R_n = R_{si}(1-\alpha)(a_7 + b_7 T_{\min,°C} + c_7 DT_{a,°C} + d_7 NDVI + e_7 RH_{\%}) + f_7 \tag{12}$$

where a_7, b_7, c_7, d_7, e_7, and f_7 are coefficients. To incorporate the contribution of elevation, $T_{min,℃}$ is corrected for sea level by decreasing the temperature by 6.5°C for each 1-km increase in elevation (Wang and Liang, 2009a). This model is the first to consider surface elevation. After validation using measurements at 24 sites worldwide, it was demonstrated that the original model (Eq. (11)) provided good estimates of the daytime R_n for all sky conditions with bias varying from 27.8 to 9.7 W m^{-2} (63% in relative value) for different sites, and RMSE from 12.8 to 21Wm^{-2} (from 15% to 19% in relative value) for different sites, and an average of 16.9 W m^{-2} (16% relative) for all sites.

Many studies have discussed whether the estimates of R_n can be improved by incorporating surface albedo in the empirical models, but no consensus has been reached. To better understand the effect of albedo, the models with R_{ns} or R_{si} (*mod3–mod7*) were modified by replacement with R_{si}, or R_{ns} (by setting albedo equal to 0 or not) respectively. Because *mod2* is the modified *mod1*, therefore, seven original linear regression models (*mod1–mod7*) and five modified models (*mod3'–mod7'*) were evaluated in the present study.

2.1.2 Cross-validation procedure for model evaluation

R_n estimation methods studied here were evaluated based on a leave-one-out cross-validation procedure. The observations from one site were used for validation and the observations from all other sites we used for model fitting. The procedure was repeated and the statistics of the validation results were compiled. Three measures were used to characterize the model performance: R^2, root mean squared error (RMSE), and bias. In general, all three measures were examined to evaluate the performance of various models, but RMSE values were given larger weighs.

2.2Data

The data used in this study comprised the in-situ radiation measurements, remote sensing products, and meteorological reanalysis data. The remote sensing products and reanalysis data were used to map net radiation on a global scale. After multiple trial experiments, no significant differences in estimated R_n with the eight models by using daily or daytime meteorological data was found. Therefore, after pre-processing with strict quality control, all of these data were aggregated to a daily scale except radiation measurements which were aggregated to a daytime scale. Further details of these data are given below.

2.2.1In-situradiation observations

(1)Measurement networks

The observed net radiation data were collected from 326 sites in 12 global measurement networks, as shown in Fig.1. These sites are distributed across the globe and represent different climatic and ecosystem conditions, which range from the Arctic to the Antarctic. Some two thirds of these sites may be ascribed to the La Thuile dataset of the FLUXNET network. Table 1 provides more information on each network.

The land cover types at these sites, as defined by the International Geosphere-Biosphere Programme (IGBP), included evergreen broadleaf forest, evergreen needle-leaf forest, deciduous broadleaf forest, deciduous needle-leaf forest, mixed forest, cropland, grassland, savanna, ice, barren or sparse vegetation, wetland and shrubland (Table 2). The elevations of these sites ranged from -0.7m to 5063m above sea level. This comprehensive representation of land cover types, widespread spatial distribution, and different elevations ensured that the global applicability of the models was assessed.

Note that some of these locations where observations of net radiation were made did not have associated meteorological measurements like air temperature, wind, etc., so that model reanalysis was needed for these variables.

(2) Daytime radiation pre-processing

The radiation measurements came from different observation networks, so various pre-processing procedures were required. It is noteworthy that the La Thuile dataset is temporally continuous because its missing data have been filled using a time-filling methods (Falge et al., 2001). However, other datasets have not been filled in this study. The observation times for each site have been transformed into the solar time for consistency, and then the radiation observations (R_n and R_{si}) were aggregated into the daytime mean values. The “daytime” in this study is defined as the time period between sunrise and sunset, so the sunrise and sunset times for each site should be determined firstly according to Doggett et al.(1978). After that, the daytime radiation values were calculated by averaging all the observations between sunrise and sunset for each site. To ensure quality control, the daytime values were only calculated if at least one observation was available in each single hour during daytime hours. Finally, all of the daytime values were checked manually, and any unreasonable values were removed.

Note that the methods proposed by Doggett et al. (1978) for estimating the sunrise and sunset times does not account for the effect of terrain on solar radiation, which may limit its applications over complex terrain.

2.2.2 Satellite products

Land surface changes can be characterized by the long time series NDVI and surface albedo, so two satellite products (*NDVI* and surface albedo) were used in this study to explore the effects of land surface characteristics on the surface net radiation estimates. To match the long term period of the radiation measurements, the bi-weekly 8-km NDVI products from 1982-2010 derived from the Advanced High Resolution Radiometer (AVHRR) data on the National Oceanic and Atmospheric Administration (NOAA) polar-orbiting satellite by the NASA Global Inventory Monitoring and Modeling Studies (GIMMS) (Tucker et al., 2005) and the 8-day 0.05° spatial resolution albedo products from 1982-2010 extracted from the Global

Land Surface Satellite (GLASS) datasets were used in this study. The AVHRR GIMMS NDVI product has been used widely (Jiang and Liang, 2013; Zhang et al., 2013), and the GLASS albedo product has been demonstrated to be more accurate than other products(Liang et al., 2013a; Liang et al., 2013c; Liu et al., 2013a; Qu et al., 2014). The NDVI and albedo time series data were extracted for each site.

For all these models discussed in Section 2.111, ground measured incident shortwave radiation data (R_{si}) and the corresponding satellite albedo product (α) for calculating R_{ns} were used in this study. However, satellite products will need to be used when applying these models to map net radiation at the global scale, which is one of the objectives in the phase-II GLASS project. GLASS shortwave radiation product (R_{si}) has 5km and 3h resolutions currently only from 2008-2010 (Liang et al., 2013a; Liang et al., 2013c; Zhang et al., 2014), but it is being extended to cover multiple years.

2.2.3 Reanalysis data

Meteorological reanalysis data were used for global mapping in the present study because of the limited coverage of the field meteorological observation networks. We used NASA Modern Era Retrospective-Analysis for Research and Applications (MERRA) data (Rienecker et al., 2011). Multiple meteorological variables, including maximum air temperature (T_{max}, °C), minimum air temperature (T_{min}, °C), mean air temperature (T_a, °C), diurnal temperature range (DT, °C), wind speed (W, m/s), and surface air pressure (PS, pa), were first extracted for each site from 1982–2010, and the hourly MERRA data were then aggregated to obtain daily values. The relative humidity ($RH_{\%}$) cannot be extracted from MERRA directly, so it was calculated from other MERRA quantities (http://www.cactus2000.de/uk/unit/masshum.shtml):

$$RH_{\%} = \frac{PS_{pa} \Big/ \left((m_{dry} qv_{kg/kg} + m_{h_2o} - m_{h_2o} qv_{kg/kg}) / (qv_{kg/kg} m_{dry}) \right)}{a_0 + T_{a,°C}(a_1 + T_{a,°C}(a_2 + T_{a,°C}(a_3 + T_{a,°C}(a_4 + T_{a,°C}(a_5 + T_{a,°C} a_6 / 1000)))))} \quad (13)$$

where PS_{pa} is the surface air pressure, and $qv_{kg/kg}$ is the specific humidity from MERRA. m_{dry} and m_{h_2o} are the molar mass of dry air and water, and they were defined as 28.9644 g/mol and 18.01534 g/mol respectively. The denominator is used for vapor pressure of water calculation (Lowe and Ficke, 1974). The other constants are defined as: $a_0 = 6.107799961$, $a_1 = 0.443651$, $a_2 = 1.4289 \times 10^{-2}$, $a_3 = 2.65 \times 10^{-4}$, $a_4 = 3.03 \times 10^{-6}$, $a_5 = 2.03 \times 10^{-8}$, and $a_6 = 6.1368 \times 10^{-8}$.

3. Results and discussion

After pre-processing, 414,540 observations were used from 326 sites during 1992–2010.The models were fitted with these observations in two cases. In case 1, the models were fitted using all the observations, i.e., *global models*. In case 2, the observations were divided into several subsets based on their surface characteristics (see Section 3.1.2) and the models obtained are referred to as *conditional models*.

3.1 Model evaluation results

3.1.1 Global model

The performances of all the empirical models based on the cross-validations are shown in Table 3. The results show that including the surface albedo generally produced better fitting results. For example, the regression statistics of *mod3* was improved, where R^2 increased from 0.823 to 0.888, RMSE decreased from 52.895 to 42.005Wm^{-2}, and bias changed from –0.069 to 0.019Wm^{-2} when R_{si} was replaced with R_{ns}. Similar improvements were obtained with *mod5*. However, the fitting accuracy declined when R_{ns} was replaced with R_{si} in *mod4*, *mod6*, *mod7* and *modnew*. Among all the models, *modnew* and *mod7* had the best performance, followed by *mod4* and *mod6*. The modified models *mod3'* and *mod5'* performed as well as *mod4* and *mod6*.

In Fig. 2 three measures of the fitting statistics (R^2, RMSE, and bias) are compared, where only the best for each model was selected (*mod1, mod2, mod3', mod4, mod5', mod6, mod7,* and *modnew*). Note that all of the models selected included R_{ns}. *Mod7* and *modnew* yielded higher R^2 values, lower RMSE, and almost zero bias. The other models delivered similar R_n fitting performance.

The coefficients of the eight global models (*mod1–modnew*) using all of the observations from 326 sites are shown in Table4. All of the dependent variables were significant ($p<0.05$). Only the best model in each case is shown in this table.

To better understand the differences in our results compared with previous studies, the original coefficients of some published models are shown in Table5, as well as their fitting statistics using all of the measurements in the present study. Although many studies employed calibrated model coefficients, some coefficients could not be used for comparison in the present study due to the different time scales employed (daily/monthly), thus only five models were selected. As earlier, only the best variants for each model are shown here, where *mod1*, *mod2*, *mod4*, and the revised *mod3* (*mod3'*–containing R_{ns}) and *mod7* (containing the bias term) were compared with the original published models. Note that the coefficients for Linacre (1992) and Iziomon et al. (2000) in Table 5 are the median coefficients from 19 sites and three sites in their studies respectively. In general, the coefficients of *mod1* and *mod2* were similar in different studies, but the model bias became smaller when more sites were used for fitting. For *mod3*, the coefficients differed considerably because R_{ns} was used in our study and it is obvious that the model fitting accuracy was improved significantly by using *mod3'*, with the RMSE of 41.81 and the bias of -0.003 Wm^{-2}. The coefficients were also different for *mod4* and the model-data mismatch was worse than that obtained using the original model. For *mod7*, the coefficients were different due to the addition of the bias term, although the bias decreased near zero using the new model. Therefore, the comparative results indicate the importance of using comprehensive measurements when fitting empirical models.

3.1.2 Conditional model

In the global model, the models had fixed coefficients for all land surfaces. Most previous studies focused on a small region or on a few sites, thus they were unable to discuss the effects of land surface on the net radiation. By contrast, the extensive observations used in the present study were collected globally (Fig.1), so it was possible for us to explore the conditional mode, i.e., fitting models in specific conditions.

After multiple trial experiments, we found that the relationships between R_{si} and R_n differed with various combinations of surface *NDVI* and albedo. The models tested in our study were all based on the relationship between R_n and shortwave radiation, so we divided the entire dataset into the subsets based on the *NDVI* and albedo according to the different relationships between R_{si} and R_n, as shown in Fig.3. Fig. 3a and 3c show the scatter plots for R_{si} and R_n with different NDVI values and their corresponding albedo histograms (Fig. 3b and 3d). An NDVI threshold of 0.2 was selected to identify vegetated surfaces that have similar albedo values. When NDVI<0.2 (no vegetation, Fig.3a), the non-vegetated surfaces (Fig.3b) were categorized into three classes: albedo≤0.25, 0.25<albedo<0.7, and albedo≥0.7, and Fig.4shows that the relationships between R_{si} and R_n differed considerably among the three classes. However, the relation between R_{si} and R_n (Fig.3c) was similar with vegetated surfaces (NDVI≥0.2). Thus, four categories were identified, as shown in Table 6.

Table 6 shows the four classification criteria and the corresponding numbers of observations for the conditional models. For simplicity, we denote the four categories as S1 (NDVI<0.2 and albedo≤0.25), S2 (NDVI<0.2 and 0.25<albedo<0.7), S3 (NDVI<0.2 and albedo ≥ 0.7), and S4 (NDVI ≥ 0.2). These four categories corresponded to some of the major land cover types found on the Earth. For example, S1 can represent wetland, S2 represents desert or barren land with sparse vegetation, S3 represents snow/ice, and S4 represents the remaining vegetation surface types. Furthermore, the seasonal information can also be represented by these categories. In the following, the performances of the eight net radiation estimation models are discussed with the four individual categories.

Similar to the global model evaluation, the performance of these models and those modified by replacing R_{si} (R_{sn}) with R_{sn} (R_{si}) were also compared based on these four categories. To eliminate the effects of NDVI values in S1–S3, the *NDVI* values were set to 0. For simplicity, only the best fitting result was selected for each model for comparison, and the final model selection results are shown in Table 7, which shows that the fitting accuracy was improved by incorporating albedo for most of the categories and empirical models, except *mod7* and *modnew* for S1.

Fig. 5 shows the comparative results for all models with the different categories. For class S1, *modnew'* yielded the best performance, followed by *mod2 and mod3'* with similar performances levels, and *mod7*' had the highest bias, although R^2 (0.775) and RMSE (55.415 Wm^{-2}) were good. For class S2, *mod2, mod3', mod6,* and *modnew* yielded similar regression accuracy, although *mod3'* was the best, whereas *mod7* only performed better than *mod1*, which had the poorest performance. However, the overall fitting accuracies for S2 were not as good as those for S1 and S4, which indicates that the use of incoming shortwave radiation for -estimating R_n is more suitable for non-vegetated surfaces with low albedo or other ordinary land surface types. Compared with the other categories, S3 was very different because there was nonlinear relationship between R_{si} and R_n (Fig. 4). Nearly all of these models had similar performance. The average R^2 was only around 0.1, but the RMSE values were very small compared to those in other cases and the biases were nearly zero. Keep in mind that net radiation of snow/ice surfaces is relatively small because of high albedo. The comparison showed that *mod2* yielded the best performance for S3. *Modnew* was the model with the best performance for S4.

Overall, several conclusions can be made based on these results: (1) the new model *modnew* that was developed in the present study had the best performance and it was very stable with the four categories; (2) unlike other models, the fitting results could not be improved by introducing albedo in *mod7* and *modnew* for class S1 (see Table 7); (3) *mod1* only used R_{si} and it yielded the worst performance in general.

In summary, all empirical net radiation fitting models that included shortwave radiation could be used for net radiation estimation in most situations because their fitting accuracy was acceptable despite some differences from each other. In particular, net radiation is difficult to estimate over a surface that has no vegetation or sparse vegetation and high albedo, thus the physically-based or longwave radiation parameterization models or non-linear models should be considered in this case.

3.2 Discussions

Previous studies of net radiation estimation models have assessed the impacts of surface albedo, air temperature, and surface elevation, but their conclusions are inconsistent and not comprehensive. In the present study, we tested these models simply by studying the relationships between the measured and simulated R_n, as well as related factors (e.g., surface albedo, NDVI, air temperature), for each model in every category (S1, S2, S3, S4 and global). Due to unavailability of cloud data, the clearness index (*CI*) was used instead. We observed that the relationships between the fitting errors and other factors were very similar for all models in each category, where the daily air mean/minimum temperature, wind speed and *CI* were the most sensitive factors during net radiation estimation. We consider *modnew* as an example.

Fig. 6a-e show the relationships between the net radiation fitting errors and the daily air mean temperature. In general, the fitting errors were greater with higher air temperature, except for classS1. Higher air temperature may correspond to a hotter season (summer), near noon local time, or low latitude, which generally have larger incident shortwave radiation and therefore net radiation. Thus, it is reasonable to have larger absolutely errors. Besides, higher air temperature also leads to larger longwave radiation.

For wind speed (Fig. 6f-j), the fitting errors were greater with smaller wind speeds, except for class S1. Weaker wind may indicate warmer air and larger incident shortwave radiation and longwave radiation. Their relative errors may not display the similar trends.

The influence of cloud was very similar for all categories. Fig. 6k-o show that the fitting errors were smaller when the sky was overcast, which is consistent with the previous findings (Alados et al., 2003; Kaminsky and Dubayah, 1997). It may be also explained by the reduced absolute magnitude of incident solar radiation under cloudy conditions.

We also studied the effects of elevation on net radiation estimation. The air temperature is usually scaled by elevation in the models, but we found that scaling the air temperature by elevation did not make much difference.

Therefore, the effects of air temperature and cloud may consider to be incorporated into the estimation models in future research because satellite remote sensing is capable of producing accurate products of air temperature and cloud coverage. Although wind cannot be accurately retrieved over land surfaces from satellite data, if our speculations discussed above are right, wind effects can be addressed if models incorporate the information of air temperature and cloud coverage.

4. Summary

Due to the inadequate spatial representation of field measurements, satellite remote sensing provides a practical method for mapping net radiation spatially and temporally at different scales. A practical solution is to estimate the net radiation empirically based on the incoming shortwave radiation or shortwave net radiation, which can be estimated accurately from satellite observations. To develop a robust empirical model, we collected as many comprehensive ground measurements as possible and evaluated the most commonly used empirical models.

We evaluated seven daytime net radiation estimation empirical models using observations obtained from 326 independent sites during 1992–2010. These sites were distributed worldwide and they represented the major land cover types on the Earth, as well as seasonal information. The leave-one-out cross-validation method was used to derive calibration coefficients and for validation. The performances of these models were evaluated using the whole dataset (*global model*) or four subsets based on the surface albedo and *NDVI* values (*conditional model*). The effects of albedo, elevation, and some meteorological factors were investigated in the present study.

Based on extensive evaluations and analyses of existing models, we developed a new model that performed better than the existing models in both the global and conditional models. In the global model, the RMSE of this new model was approximately 40.0 Wm^{-2}. In the conditional mode, the new model could reduce the RMSEs to 53.92, 50.99, 18.23, and 39.01 Wm^{-2} for S1–S4, respectively, which were better results than those obtained using most of the other linear empirical models considered in this study.

Noting that these models evaluated in this study are linear based on the linear relationships between all-wave net radiation and incident surface shortwave radiation or surface shortwave net radiation, but the possible non-linear relations have not been considered here but presented elsewhere (Jiang et al. 2014).The global distribution of the observations used in this study is largely biased toward the boreal regions and western countries, and few urban sites were included. And also the terrain slope and orientation of these radiation measurements have not been taken into account in this study. Besides, the remotely sensed and reanalysis data used have coarser spatial resolution, and may not be the best to match the site radiation observations. All these aspects need to be addressed in the future.

Acknowledgements

This study was funded partly by the National High-Technology Research and Development Program of China under Grant 2013AA122800, the Fundamental Research Funds for the Central Universities (ID: 2013NT28), and the Natural Science Foundation of China (No. 41401381 and No. 41331173). This work used eddy covariance data acquired by the FLUXNET community and in particular by the following networks: AmeriFlux (U.S. Department of Energy, Biological and Environmental Research, Terrestrial Carbon Program (DE-FG02-04ER63917)), AfriFlux, AsiaFlux, CarboAfrica, CarboEuropeIP, CarboItaly, CarboMont, ChinaFlux, Fluxnet-Canada (supported by CFCAS, NSERC, BIOCAP, Environment Canada, and NRCan), GreenGrass, KoFlux, LBA, NECC, OzFlux, TCOS-Siberia, USCCC. We acknowledge the financial support to the eddy covariance data harmonization provided by CarboEuropeIP, FAO-GTOS-TCO, Ileaps, Max Planck Institute for Biogeochemistry, National Science Foundation, University of Tuscia, Université Laval, Environment Canada and US Department of Energy and the datasets development and technical support from Berkeley Water Center, Lawrence Berkeley National Laboratory, Microsoft Researche Science, Oak Ridge National Laboratory, University of California – Berkeley and the University of Virginia. We also would like to thank other radiation measurements providers (their names are listed in Table 1). In particular, we thank Dr. Yan Li and Dr. Ran Li from the Xinjiang Institute of Ecology and Geography, CAS, and Dr. Jean Christophe Calvet from CNRM-GAME for sharing their data. We would like to thank two anonymous reviewers for their valuable comments and suggestions that have greatly improved the presentation of this paper.

References

Al-Riahi, M., Al-Jumaily, K. and Kamies, I., 2003. Measurements of net radiation and its components in semi-arid climate of Baghdad. Energy Conversion and Management, 44(4): 509-525.

Alados, I., Foyo-Moreno, I., Olmo, F.J. and Alados-Arboledas, L., 2003. Relationship between net radiation and solar radiation for semi-arid shrub-land. Agricultural and Forest Meteorology, 116(3-4): 221-227.

Allen, R. et al., 2011. Satellite-based ET estimation in agriculture using SEBAL and METRIC. Hydrological Processes, 25(26): 4011-4027.

Allen, R.G., Pereira, L.S., Raes, D. and Smith, M., 1998. Crop evapotranspiration-Guidelines for computing crop water requirements-FAO Irrigation and drainage paper 56. FAO, Rome, 300: 6541.

Augustine, J.A., DeLuisi, J.J. and Long, C.N., 2000. SURFRAD—A National Surface Radiation Budget Network for Atmospheric Research. Bulletin of the American Meteorological Society, 81(10): 2341-2357.

Augustine, J.A., Hodges, G.B., Cornwall, C.R., Michalsky, J.J. and Medina, C.I., 2005. An Update on SURFRAD—The GCOS Surface Radiation Budget Network for the Continental United States. Journal of Atmospheric and Oceanic Technology, 22(10): 1460-1472.

Bisht, G. and Bras, R.L., 2011. Estimation of Net Radiation From the Moderate Resolution Imaging Spectroradiometer Over the Continental United States. IEEE transactions on geoscience and remote sensing, 49(6): 2448-2462.

de Rosnay, P. et al., 2006. SMOSREX: A long term field campaign experiment for soil moisture and land surface processes remote sensing. Remote Sensing of Environment, 102(3–4): 377-389.

Doggett, L., Kaplan, G. and Seidelmann, P., 1978. Almanac for computers, 1978. Nautical Almanac Office, United States Naval Observatory, Washington DC, USA, pp. B5.

Falge, E. et al., 2001. Gap filling strategies for defensible annual sums of net ecosystem exchange. Agricultural and Forest Meteorology, 107(1): 43-69.

Gao, Y., Long, D. and Li, Z.-L., 2008. Estimation of daily actual evapotranspiration from remotely sensed data under complex terrain over the upper Chao river basin in North China. International Journal of Remote Sensing, 29(11): 3295-3315.

Holtslag, A. and Van Ulden, A., 1983. A simple scheme for daytime estimates of the surface fluxes from routine weather data. Journal of Climate and Applied Meteorology, 22(4): 517-529.

Hwang, K., Choi, M., Lee, S. and Seo, J.-W., 2012. Estimation of instantaneous and daily net radiation from MODIS data under clear sky conditions: a case study in East Asia. Irrigation Science: 1-12.

Irmak, S., Irmak, A., Jones, J., Howell, T., Jacobs, J., Allen, R., and Hoogenboom, G., 2003. Predicting Daily Net Radiation Using Minimum Climatological Data. Journal of Irrigation and Drainage Engineering, 129(4): 256-269.

Iziomon, M.G., Mayer, H. and Matzarakis, A., 2000. Empirical Models for Estimating Net Radiative Flux: A Case Study for Three Mid-Latitude Sites with Orographic Variability. Astrophysics and Space Science, 273(1): 313-330.

Jia, Z.Z., Liu, S.M., Xu, Z.W., Chen, Y.J. and Zhu, M.J., 2012. Validation of remotely sensed evapotranspiration over the Hai River Basin, China. Journal of Geophysical Research-Atmospheres, 117.

Jiang, B., Zhang, Y., Liang, S.L., Zhang X.T., and Xiao, Z.Q., 2014. Surface Daytime Net Radiation Estimation Using Artificial Neural Networks. Remote Sensing, 6: 11031-11050.

Jiang, B. and Liang, S.L., 2013. Improved vegetation greenness increases summer atmospheric water vapor over Northern China. Journal of Geophysical Research: Atmospheres, 118: 1-11.

Kaminsky, K.Z. and Dubayah, R., 1997. Estimation of surface net radiation in the boreal forest and northern prairie from shortwave flux measurements. Journal of Geophysical Research-Atmospheres, 102(D24): 29707-29716.

Kjaersgaard, J., Cuenca, R., Plauborg, F. and Hansen, S., 2007. Long-term comparisons of net radiation calculation schemes. Boundary-Layer Meteorology, 123(3): 417-431.

Kjaersgaard, J.H. et al., 2009. Comparison of the performance of net radiation calculation models. Theoretical and Applied Climatology, 98(1-2): 57-66.

Liang, S., Zhao, X., Liu, S.H., Yuan, W.P., Cheng, X., Xiao, Z.Q., Zhang, X.T., Liu, Q., Cheng, J., Tang, H.R., Qu, Y.H., Bo, Y.C., Qu, Y., Ren, H.Z., Yu, K., and Townshend, J., 2013a. A long-term Global LAnd Surface Satellite (GLASS) data-set for environmental studies. International Journal of Digital Earth, 6(sup1): 5-33.

Liang, S., Zheng, T., Liu, R., Fang, H., Tsav, S.C., and Running, S., 2006. Mapping incident Photosynthetically Active Radiation (PAR) from MODIS Data. Journal of Geophysical Research - Atmoshperes, 111, Art. No. D15208.

Liang, S.L., Wang, K.C., Zhang, X.T. and Wild, M., 2010. Review on Estimation of Land Surface Radiation and Energy Budgets From Ground Measurement, Remote Sensing and Model Simulations. Selected Topics in Applied Earth Observations and Remote Sensing, IEEE Journal of, 3(3): 225-240.

Liang, S.L., Zhang, X.T., He, T., Cheng, J. and Wang, D.D., 2013b. Remote sensing of earth surface radiation budget. In: G.P. Petropoulos (Editor), Remote Sensing of Land Surface Turbulent Fluxes and Soil Surface moisture Content: State of the Art. CRC Press, pp. 125-165.

Liang, S.L., Zhang, X.T., Xiao, Z.Q., Cheng, J., Liu, Q., and Zhao, X., 2013c. Global LAnd Surface Satellite (GLASS) products: Algorithms, Validation and Analysis. Springer.

Linacre, E., 1992. Climate data and resources: a reference and guide.

Liu, Q., Wang, L.Z., Qu, Y., Liu, N.F., Liu, S.H., Tang, H.R., and Liang, S.L., 2013a. Preliminary evaluation of the long-term GLASS albedo product. International Journal of Digital Earth, 6: 69-95.

Liu, S.M., Xu, Z.W., Wang, W.Z., Jia, Z.Z., Zhu, M.J., Bai, J., and Wang, J.M., 2011. A comparison of eddy-covariance and large aperture scintillometer measurements with respect to the energy balance closure problem. Hydrology and Earth System Sciences, 15(4): 1291-1306.

Liu, S.M., Xu, Z.W., Zhu, Z.L., Jia, Z.Z. and Zhu, M.J., 2013b. Measurements of evapotranspiration from eddy-covariance systems and large aperture scintillometers in the Hai River Basin, China. Journal of Hydrology, 487(0): 24-38.

Long, D., Gao, Y. and Singh, V.P., 2010. Estimation of daily average net radiation from MODIS data and DEM over the Baiyangdian watershed in North China for clear sky days. Journal of Hydrology, 388(3–4): 217-233.

Lowe, P.R. and Ficke, J.M., 1974. The computation of saturation vapor pressure, DTIC Document.

Lu, J., Tang, R.L., Tang, H.J., Li, Z.L., Zhou, G.Q., Shao, K., Bi, Y.Y., and Labed, J., 2014. Daily Evaporative Fraction Parameterization Scheme Driven by Day-Night Differences in Surface Parameters: Improvement and Validation. Remote Sensing, 6(5): 4369-4390.

Lu, J., Tang, R.L., Tang, H.J. and Li, Z.L., 2013. Derivation of Daily Evaporative Fraction Based on Temporal Variations in Surface Temperature, Air Temperature, and Net Radiation. Remote Sensing, 5(10): 5369-5396.

Male, D. and Granger, R., 1981. Snow surface energy exchange. Water Resources Research, 17(3): 609-627.

Monteith, J.L., 1965. Evaporation and environment, Symposia of the Society for Experimental Biology pp. 205-224.

Monteith, J.L. and Unsworth, M.H., 1990. Principles of Environmental Physics. Edward Arnold, London, UK, pp. 291.

Ohmura, A., Gilgen, H., Hegner, H., Müller, G., Wild, M., Dutton, E.G., Forgan, B., Fröhlich, C., Philipona, R., Heimo, A., König-Langlo, G., McArthur, B., Pinker, R., Whitlock, C.H., and Dehne, K., 1998. Baseline Surface Radiation Network (BSRN/WCRP): New Precision Radiometry for Climate Research. Bulletin of the American Meteorological Society, 79(10): 2115-2136.

Qu, Y., Liu, Q., Liang, S.L., Wang, L.Z., Liu, N.F., and Liu, S.H., 2014. Improved mapping daily land-surface broadband albedo from MODIS data. IEEE Geoscience and Remote Sensing Letters, 52: 907-919.

Rienecker, M.M., Suarez M.J., Gelaro R., Todling R., Bacmeister J., Liu E., Bosilovich M.G., Schubert S.D., Takacs L., Kim G.K., Bloom S., Chen J.Y., Collins D., Conaty A., Da Silva A., Gu W., Joiner J., Koster R.D., Lucchesi R., Molod A., Owens T., Pawson S., Pegion P., Redder C.R., Reichle R., Robertson F.R., Ruddick A.G., Sienkiewicz M., and Wollen J., 2011. MERRA: NASA's Modern-Era Retrospective Analysis for Research and Applications. Journal of Climate, 24(14): 3624-3648.

Sentelhas, P.C. and Gillespie, T.J., 2008. Estimating hourly net radiation for leaf wetness duration using the Penman-Monteith equation. Theoretical and Applied Climatology, 91(1): 205-215.

Steffen, K., Box, J. and Abdalati, W., 1996. Greenland climate network: GC-Net. US Army Cold Regions Reattach and Engineering (CRREL), CRREL Special

Report: 98-103.

Swinbank, W.C., 1963. Longwave radiation from clear skies. QJR Meteorol Soc, 89: 339-348.

Tang, B. and Li, Z.-L., 2008. Estimation of instantaneous net surface longwave radiation from MODIS cloud-free data. Remote Sensing of Environment, 112(9): 3482-3492.

Tang, B., Li, Z.-L. and Zhang, R., 2006. A direct method for estimating net surface shortwave radiation from MODIS data. Remote Sensing of Environment, 103(1): 115-126.

Tucker, C.J., Pinzon J.E., Brown M.E., Slayback D.A., Pak E.W., Mahoney R., Vermote E.F., and El Saleous N., 2005. An extended AVHRR 8-km NDVI dataset compatible with MODIS and SPOT vegetation NDVI data. International Journal of Remote Sensing, 26(20): 4485-4498.

Wang, K. and Liang, S., 2009a. Estimation of Daytime Net Radiation from Shortwave Radiation Measurements and Meteorological Observations. Journal of Applied Meteorology and Climatology, 48(3): 634-643.

Wang, K.C. and Liang, S.L., 2008. An improved method for estimating global evapotranspiration based on satellite determination of surface net radiation, vegetation index, temperature, and soil moisture. Journal of Hydrometeorology, 9(4): 712-727.

Wang, W.H. and Liang, S.L., 2009b. Estimation of high-spatial resolution clear-sky longwave downward and net radiation over land surfaces from MODIS data. Remote Sensing of Environment, 113(4): 745-754.

Wu, W., Hall, C.A.S., Scatena, F.N. and Quackenbush, L.J., 2006. Spatial modelling of evapotranspiration in the luquillo experimental forest of puertorico using remotely-sensed data. J. Hydrol., 328: 733-752.

Xu, Z.W., Liu S.M., Li X., Shi S.J, Wang J.M., Zhu Z.L., Xu T.R., Wang W.Z., and Ma M.G., 2013. Intercomparison of surface energy flux measurement systems used during the HiWATER-MUSOEXE. Journal of Geophysical Research-Atmospheres, 118(23): 13140-13157.

Zhang, G., Zhang, Y., Dong, J. and Xiao, X., 2013. Green-up dates in the Tibetan Plateau have continuously advanced from 1982 to 2011. Proceedings of the National Academy of Sciences of the United States of America, 110(11): 4309-4314.

Zhang, X., Liang, S., Zhou, G.S., Wu, H. and Zhao, X., 2014. Generating Global LAnd Surface Satellite incident shortwave radiation and photosynthetically active radiation products from multiple satellite data. Remote Sensing of Environment, 152: 318-332.

Tables

Table 1 Information related to the 12 observation networks

Network/ Program	No. of sites	Time Period	Instrument	URL
Global Fluxnet (La Thuile dataset)	207	1991-2008	Kipp&ZonenCNR-1, etc.	http://www.fluxdata.org/
AsiaFlux	19	1999-2008	Kipp&Zonen CNR-1	http://www.asiaflux.net/
ARM	22	2002-2013	Kipp&Zonen CNR-1	https://www.arm.gov/
BSRN	6	1992-2012	Eppley, PIR/Kipp&Zonen CG4	http://www.bsrn.awi.de/
SURFRAD	7	1995-2012	Eppley, PIR	http://www.esrl.noaa.gov/gmd/grad/surfrad/
GAME/AAN	10	1997-2003	EKO MS0202F	http://aan.suiri.tsukuba.ac.jp/aan.html
BOREAS	5	1993-1996	Kipp&Zonen CM-5	http://daac.ornl.gov/BOREAS/bhs/BOREAS_Home.html
GC-Net	13	1995-2012	Li Cor Photodiode & REBS Q* 7	http://cires.colorado.edu/science/groups/steffen/gcnet/
CEOP-GEWEX	37	2002-2009	Eppley, PIR/Kipp&Zonen CG4	http://www.eol.ucar.edu/projects/ceop/
CEOP	10	2007-2009		
SMOSREX	1	2005-2010	Kipp&Zonen CNR-1	http://www.cesbio.ups-tlse.fr/us/smos/smos_lewis.html
CERN	1	2007		http://www.cerndata.ac.cn/

ARM: Atmospheric Radiation Measurement, BSRN: Baseline Surface Radiation Network(Ohmura et al., 1998), SURFRAD: Surface Radiation Network(Augustine et al., 2000; Augustine et al., 2005), BOREAS: Boreal Ecosystem-Atmosphere Study, GC-Net: Greenland Climate Network(Steffen et al., 1996), CEOP-GEWEX: Coordinated Enhanced Observing Period, CEOP: Coordinated Enhanced Observation Network of China (Jia et al., 2012; Liu et al., 2011; Liu et al., 2013b; Xu et al., 2013), SMOSREX: Surface Monitoring Of Soil Reservoir Experiment(de Rosnay et al., 2006), CERN: Chinese Ecosystem Research Network.

Table 2 Number of sites for each IGBP land cover type

IGBP Land Cover Types	**No. of sites**
Barren& Sparse vegetation	6
Cropland	50
Deciduous Broadleaf Forest	35
Deciduous Needleleaf Forest	6
Evergreen Broadleaf Forest	17
Evergreen Needleleaf Forest	68
Grassland	70
Ice	17
Mixed Forest	14
Savanna	7
Shrubland	18
Wetland	18
Total	326

Table 3 Comparative fitting statistics for seven daytime net radiation estimation models. The coefficients *a* and *b* are the slope and intercept of the linear regression relationship between estimated and measured R_n.

	a	***b*** $(W\ m^{-2})$	$\mathbf{R^2}$	**RMSE** $(W\ m^{-2})$	**bias** $(W\ m^{-2})$		***a***	***b*** $(W\ m^{-2})$	R^2	**RMSE** $(W\ m^{-2})$	**bias** $(W\ m^{-2})$
mod1	0.9991	0.167	0.767	60.634	-0.0003						
*mod2**	0.9996	0.059	0.879	43.658	-0.016						
mod3	0.9992	0.083	0.823	52.895	-0.069	*mod3'**	0.9990	0.207	0.888	42.005	0.019
*mod4**	0.9992	0.135	0.886	42.385	0.018	*mod4'*	0.9989	0.098	0.827	52.361	0.1003
mod5	0.9990	0.048	0.828	52.114	0.143	*mod5'**	0.9994	0.088	0.887	42.209	-0.028
*mod6**	0.9991	0.163	0.890	41.641	0.002	*mod6'*	0.9991	0.095	0.826	52.474	-0.077
*mod7**	0.9986	0.209	0.899	39.882	-0.045	*mod7'*	0.9984	0.250	0.867	45.901	-0.045
modnew	0.9987	0.183	0.899	40.025	-0.047	*modnew'*	0.9992	0.044	0.859	47.276	-0.098

' denotes a modified model, and * denotes models that included R_{ns}.

Table 4 Coefficients for the best eight global models

Model	Coefficients					
mod1	a_1	b_1				
	0.654	-20.317				
*mod2**	a_2	b_2				
	0.781	-13.596				
*mod3'**	a_3	b_3	c_3			
	0.867	-81.483	6.310			
*mod4**	a_4	b_4	c_4			
	0.724	0.211	-77.253			
*mod5'**	a_5	b_5	c_5	d_5		
	0.721	0.777	-301.420	296.842		
*mod6**	a_6	b_6	c_6			
	0.863	-90.491	87.219			
*mod7**	a_7	b_7	c_7	d_7	e_7	f_7
	0.5515	0.0027	0.0015	0.1321	0.1652	-10.7575
*modnew**	a_{new}	b_{new}	c_{new}	d_{new}	e_{new}	
	0.862	-65.435	24.564	54.351	20.966	

' denotes a modified model, and * denotes models that included R_{ns}.

Table 5 Comparisons of the coefficients and performance using *mod1*, *mod2*, *mod3*, *mod4*, and *mod7* in the present study and the original published reports.

	Coefficients			Model comparison		
				R^2	RMSE (Wm^{-2})	bias (Wm^{-2})
mod1	a_1	b_1		0.767	60.425	-0.0097
	0.654	-20.317				
Linacre (1992)	0.63	-23		0.769	60.425	-10.118
Iziomon et al. (2000)	0.63	-25.7		0.769	60.425	-12.818
mod2	a_2	b_2		0.880	43.511	0.001
	0.781	-13.596				
Iziomonet al. (2000)	0.80	-24.5		0.880	43.511	-6.104
mod3'	a_3	b_3	c_3	0.889	41.810	-0.003
	0.867	-81.483	6.310			
*Iziomon et al.(2000)**	0.77	-147.5	-6	0.817	53.829	-24.575
mod4	a_4	b_4	c_4	0.888	42.170	-0.008

	0.724	0.211	-77.253						
Iziomon et al.(2000)	0.82	0.028	38.4				0.882	43.200	72.230
mod7	a_7	b_7	c_7	d_7	e_7	f_7	0.902	39.356	-0.049
	0.5515	0.0027	0.0015	0.1321	0.1652	-10.7575			
Wang and Liang(2009a)	0.5129	0.0025	0.0000	0.1401	0.2604		0.899	39.883	13.251

* denotes the models that included R_{si}, where the others included R_{ns}.

Table 6 Four classification categories based on the combination of NDVI and albedo, with their corresponding numbers of observations.

Class	Classification criteria	No. of Observations
S1	NDVI<0.2 and albedo≤0.25	19111
S2	NDVI<0.2 and 0.25<albedo<0.7	17909
S3	NDVI<0.2 and albedo≥0.7	20229
S4	NDVI≥0.2	357291

Table 7 Final models selected for comparison for each category.

	Selected models
S1	mod1, mod2*, mod3'*, mod4*, mod5'*, mod6*, $mod7'_{ndvi=0}$, $modnew'_{ndvi=0}$
S2	mod1, mod2*, mod3'*, mod4*, mod5'*, mod6*, $mod7^{*}_{ndvi=0}$, $modnew^{*}_{ndvi=0}$
S3	mod1, mod2*, mod3'*, mod4*, mod5'*, mod6*, $mod7^{*}_{ndvi=0}$, $modnew^{*}_{ndvi=0}$
S4	mod1, mod2*, mod3'*, mod4*, mod5'*, mod6*, mod7*, modnew*

' denotes a modified model, and * denotes the models that included R_{ns}.

Figure Caption

Figure 1 Distribution of 326 observation sites in 12 measurement networks.

Figure 2 Comparisons of the fitting statistics for the eight selected models (*mod1*, *mod2, mod3', mod4, mod5', mod6, mod7,* and *modnew)* using three measures: (a) R^2, (b) RMSE (Wm^{-2}), (c) bias (Wm^{-2}).

Figure 3 Scatter plots for R_n and R_{si} (a, c), and their corresponding histograms of albedo (b, d) when NDVI<0.2 and NDVI≥0.2.

Figure 4 The scatter plot for R_n and R_{si} when classified by albedo whenever NDVI<0.2.

Figure 5 Comparison of the fitting accuracies (R^2, RMSE, bias) for eight selected models with four categories: (a)-(c) S1, (d)-(f) S2, (g)-(i) S3, and (j)-(l) S4.

Figure 6 Scatter plots showing the differences between the measured and model calculated R_n and related factors for each model in the five categories (S1, S2, S3, S4 and global): (a)-(e) daily mean air temperature (T), (f)-(j) daily mean wind speed (W), and (k)-(o) clearness index (CI). Positive values mean that the model underestimated net radiation.

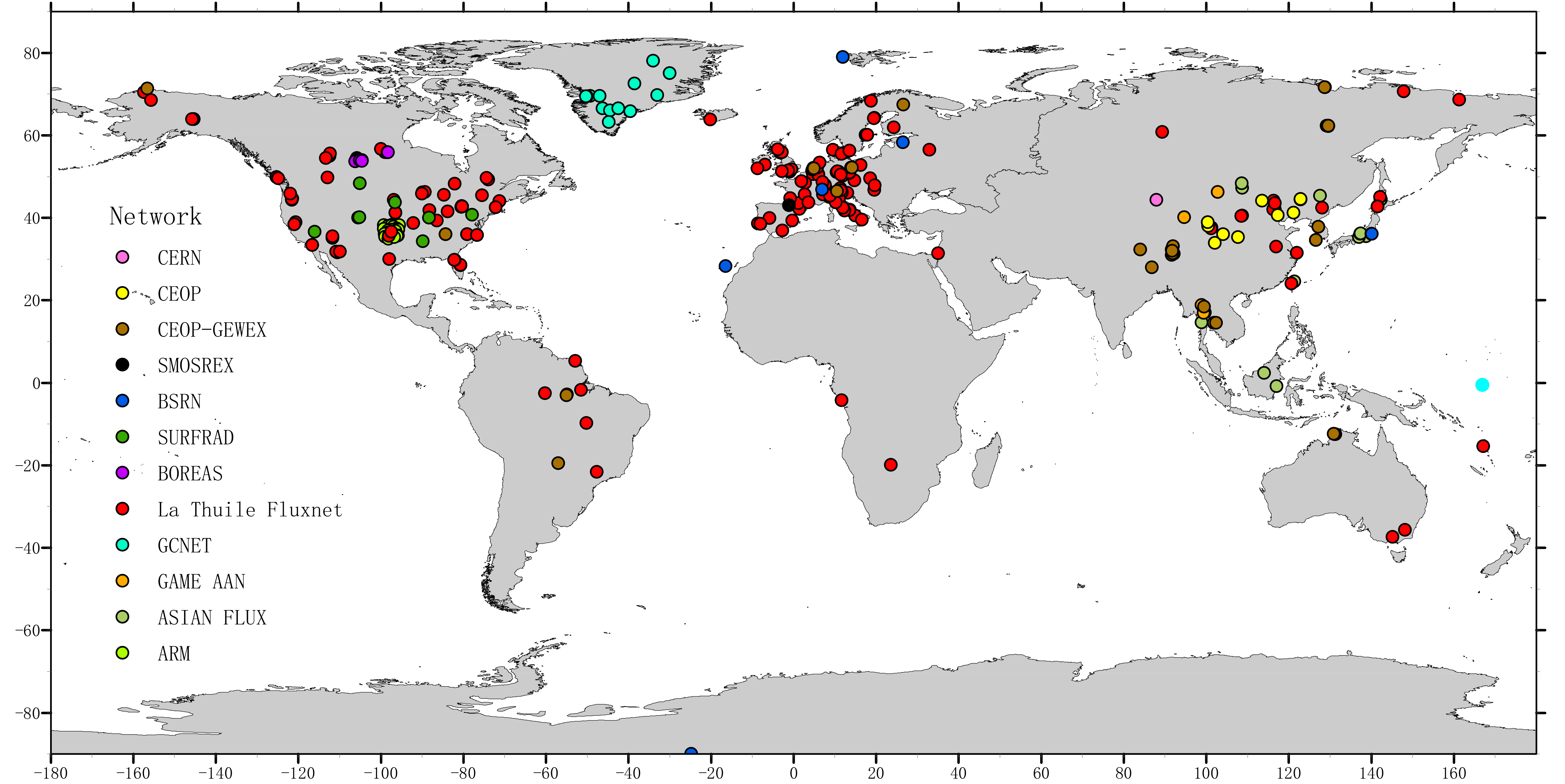
Network
CERN
CEOP
CEOP-GEWEX
SMOSREX
BSRN
SURFRAD
BOREAS
La Thuile Fluxnet
GCNET
GAME AAN
ASIAN FLUX
ARM
80
60
40
20
0
-20
-40
-60
-80
-180
-160
-140
-120
-100
-80
-60
-40
-20
0
20
40
60
80
100
120
140
160

2D Graph 5

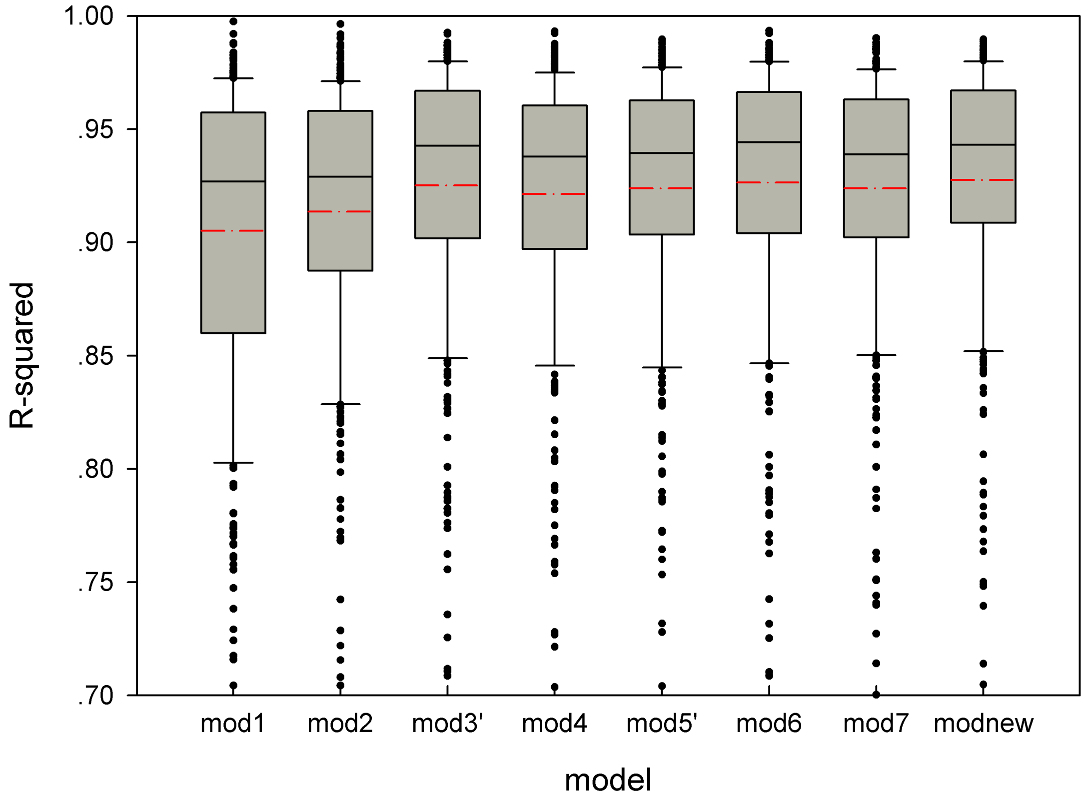

1.00
.95
.90
.85
.80
.75
.70
R-squared
mod1
mod2
mod3'
mod4
mod5'
mod6
mod7
modnew
model

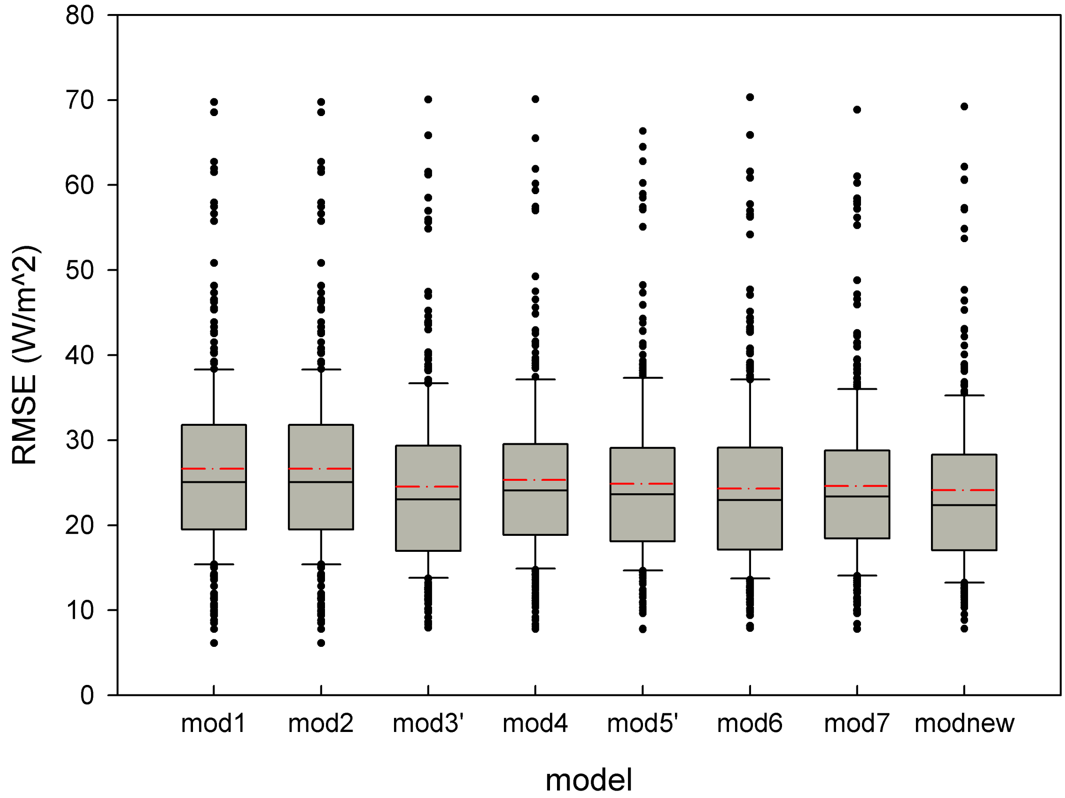

80
70
60
50
40
30
20
10
0
RMSE (W/m^2)
mod1
mod2
mod3'
mod4
mod5'
mod6
mod7
modnew
model

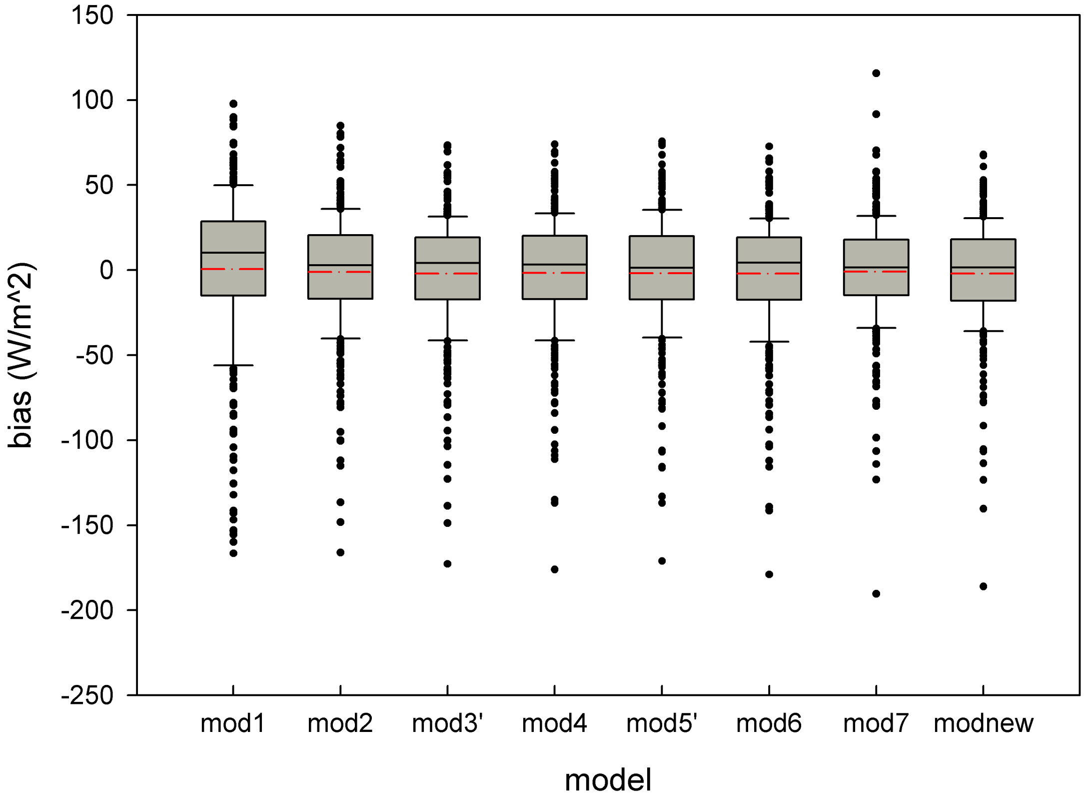

150
100
50
0
-50
-100
-150
-200
-250
bias (W/m^2)
mod1
mod2
mod3'
mod4
mod5'
mod6
mod7
modnew
model

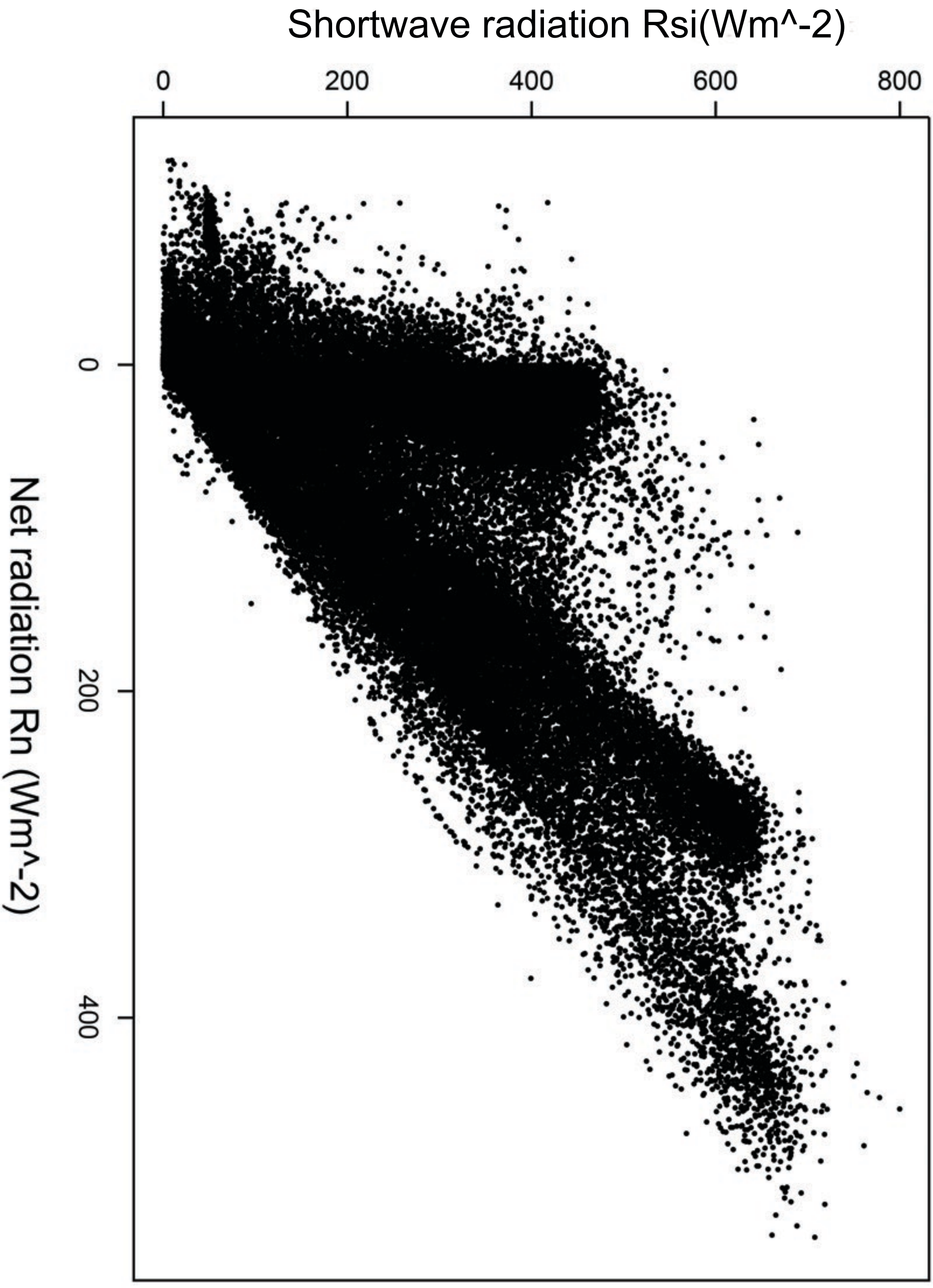

Shortwave radiation Rsi(Wm^-2)
0
200
400
600
800
Net radiation Rn (Wm^-2)
0
200
400

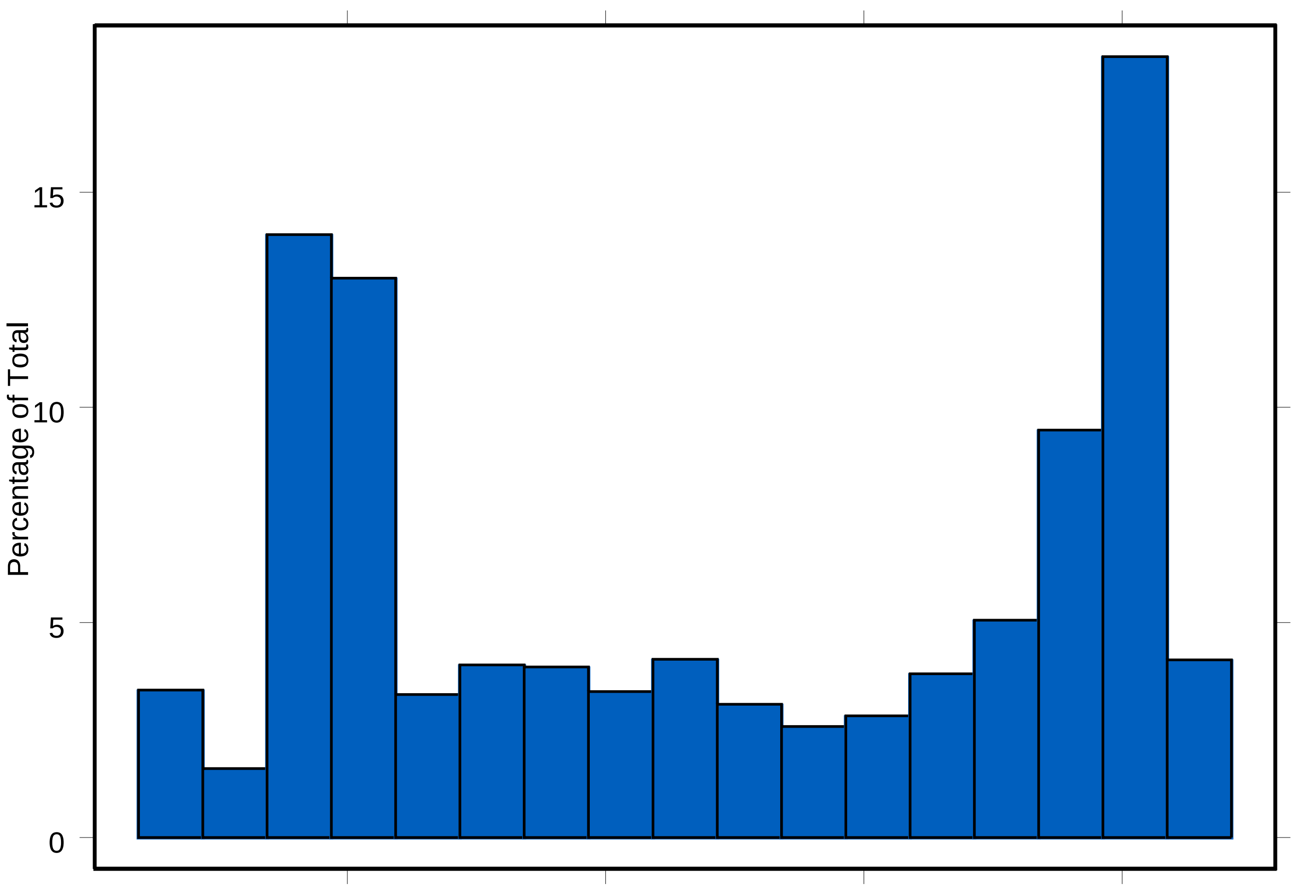

Percentage of Total
15
10
5
0
0.2
0.4
0.6
0.8
albedo

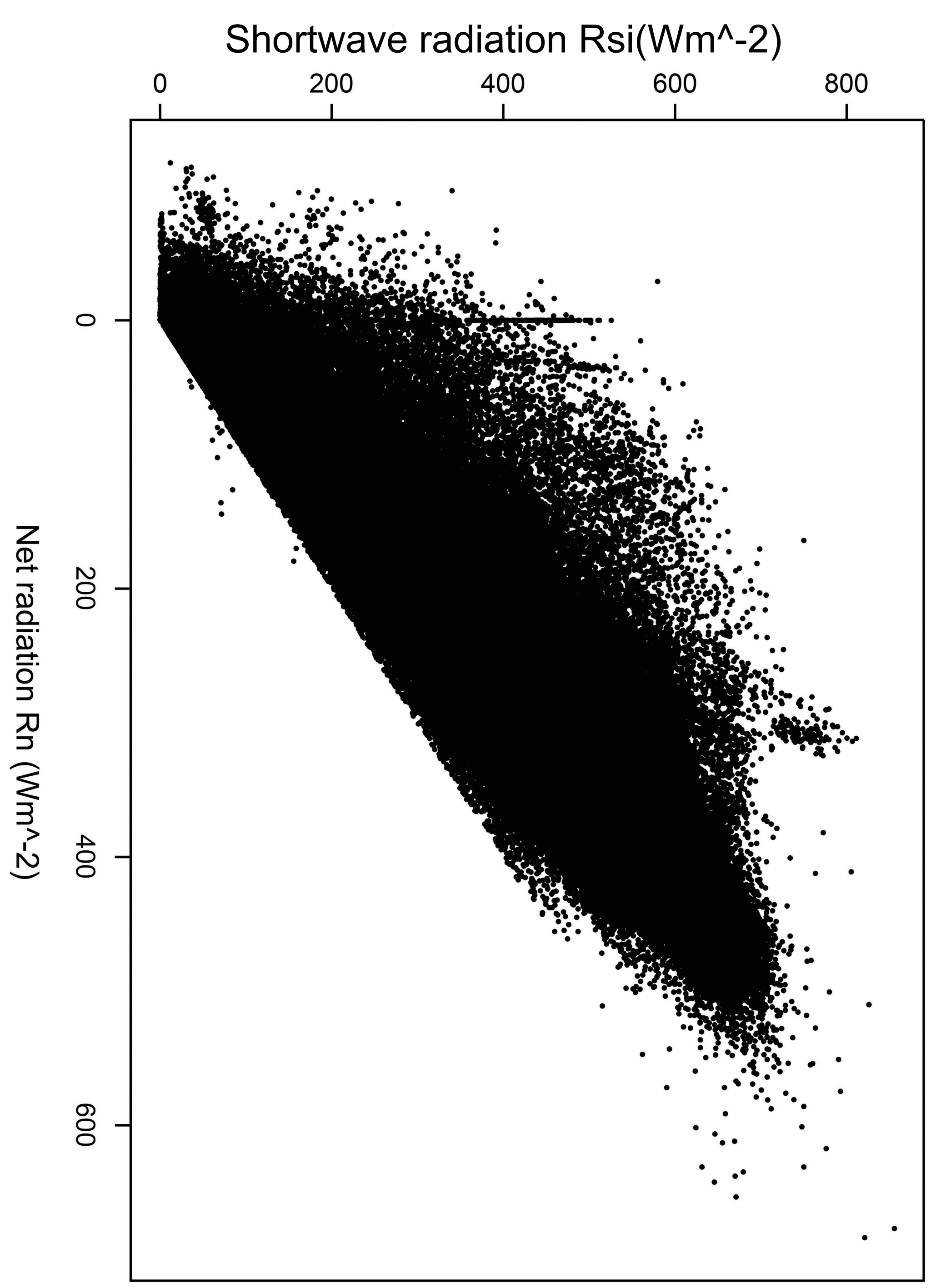

Shortwave radiation Rsi(Wm^-2)
0
200
400
600
800
Net radiation Rn (Wm^-2)
0
200
400
600

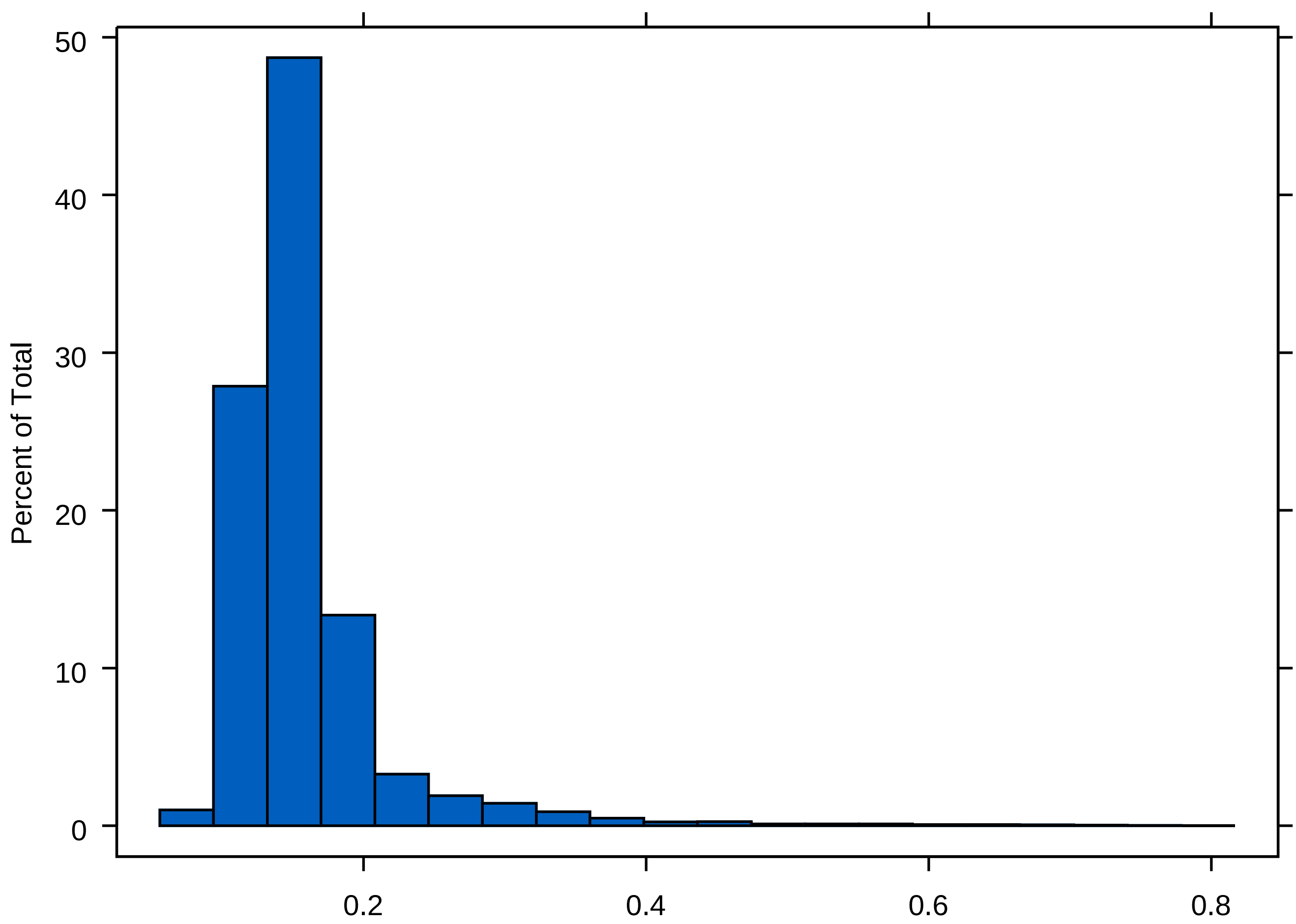

Percent of Total
0
10
20
30
40
50
0.2
0.4
0.6
0.8
albedo

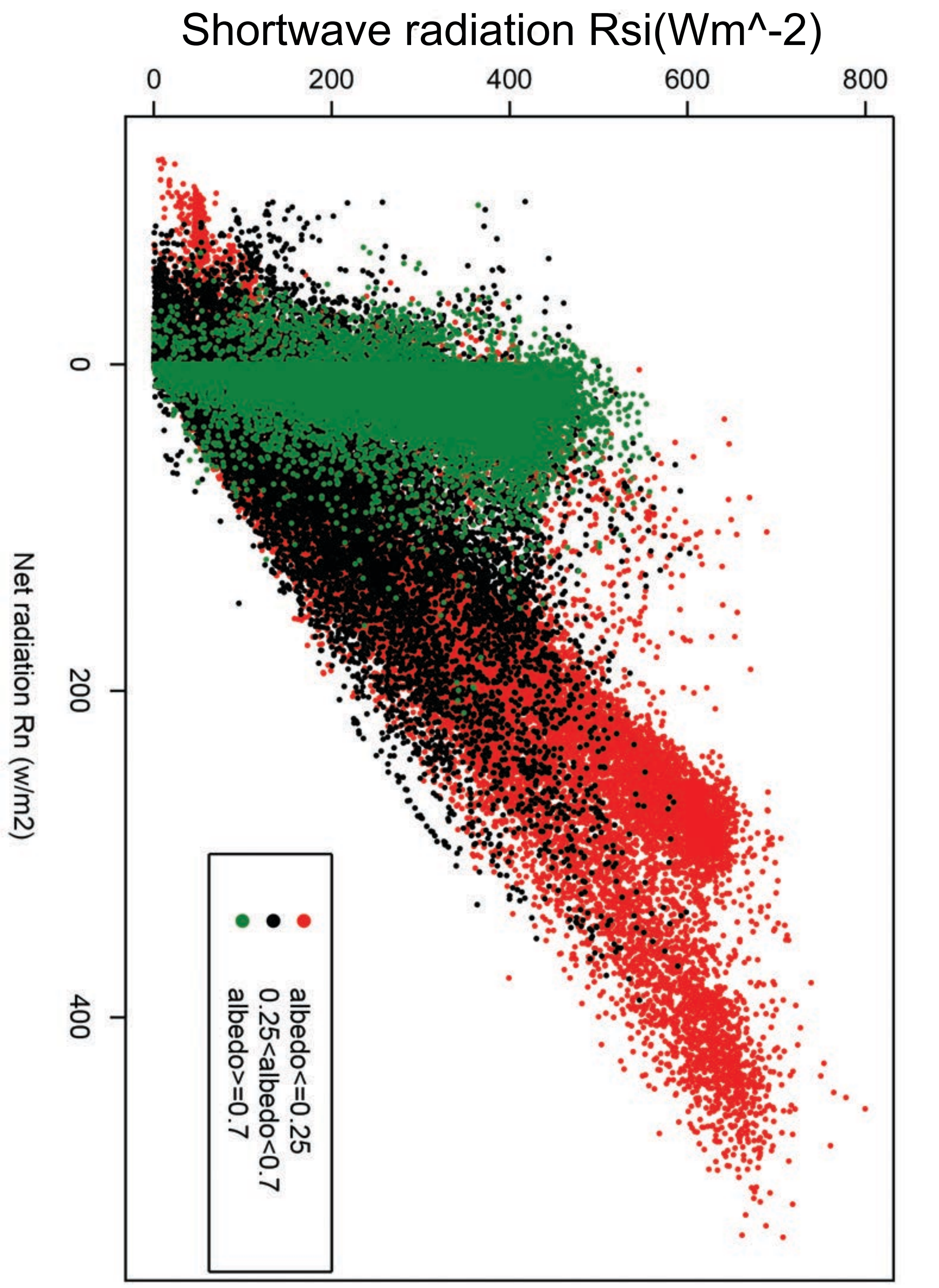
Shortwave radiation Rsi(Wm^-2)
0
200
400
600
800
Net radiation Rn (w/m2)
0
200
400
albedo<=0.25
0.25<albedo<0.7
albedo>=0.7

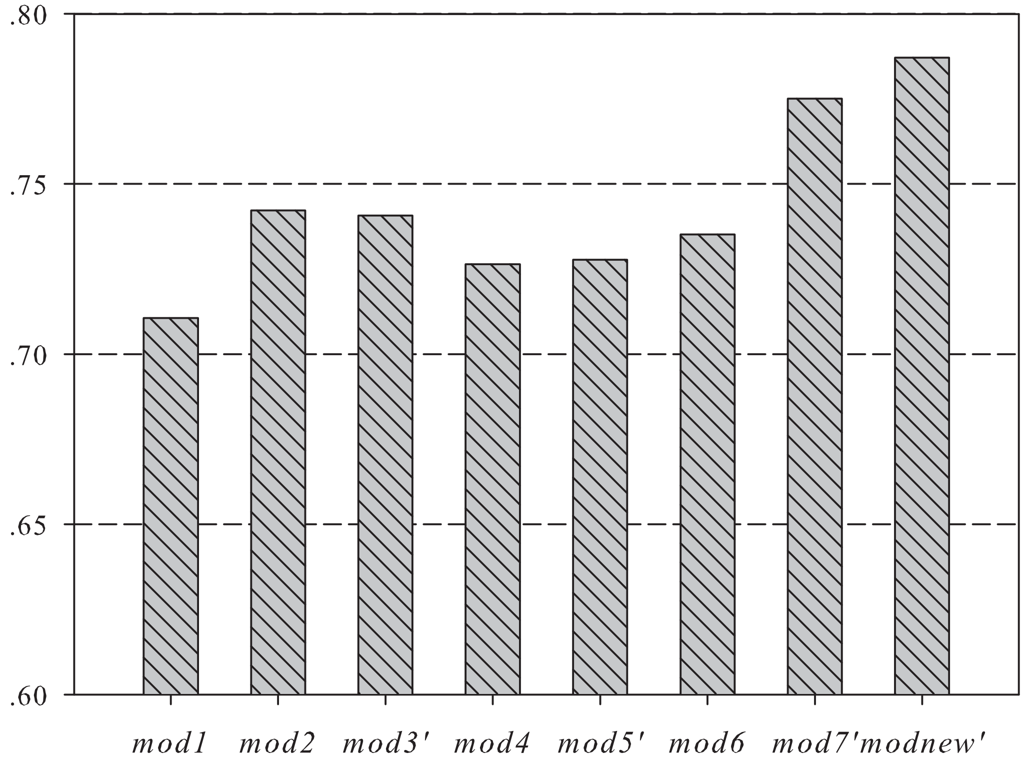

.80
.75
.70
.65
.60
mod1
mod2
mod3'
mod4
mod5'
mod6
mod7'
modnew'

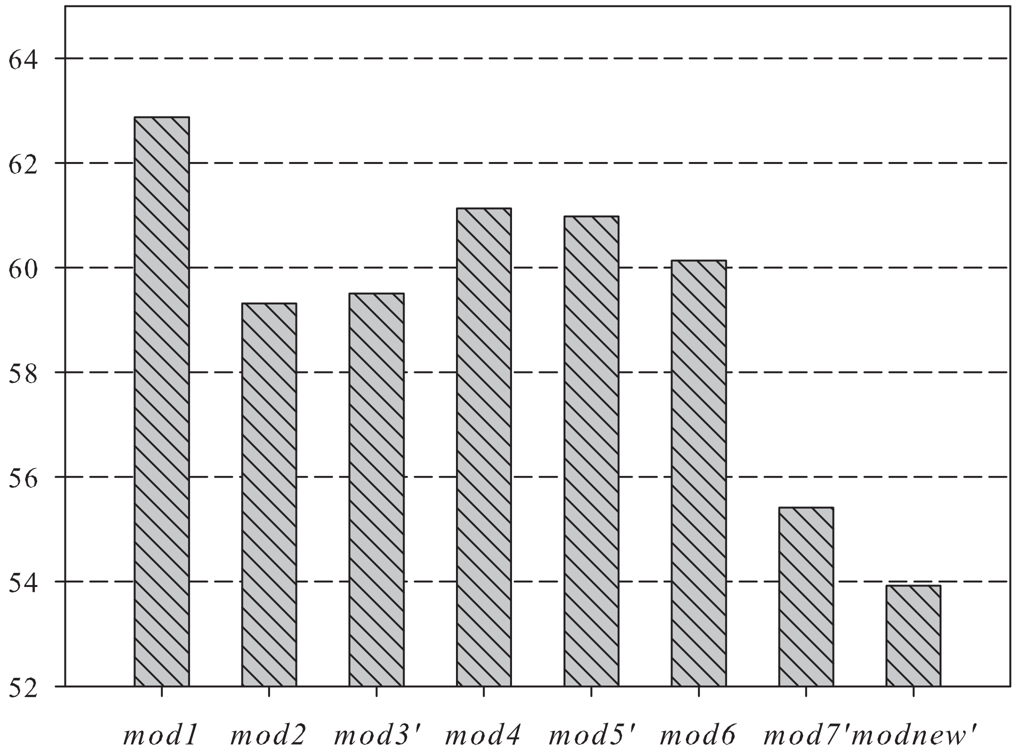
64
62
60
58
56
54
52
mod1
mod2
mod3'
mod4
mod5'
mod6
mod7'
modnew'

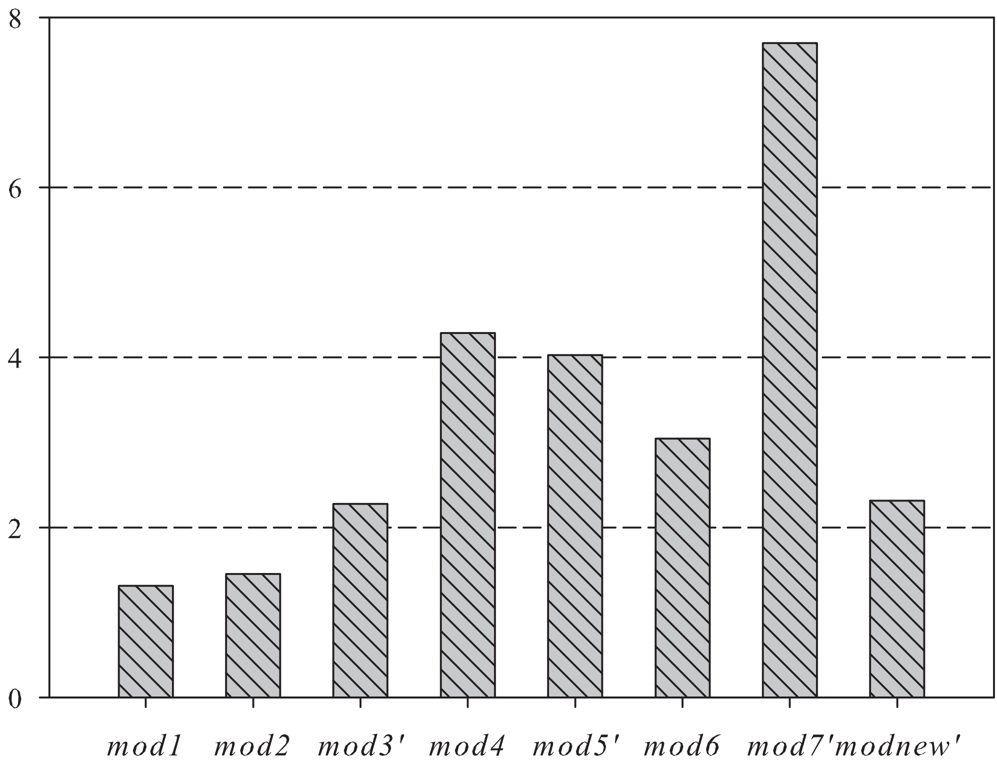
8
6
4
2
0
mod1
mod2
mod3'
mod4
mod5'
mod6
mod7'
modnew'

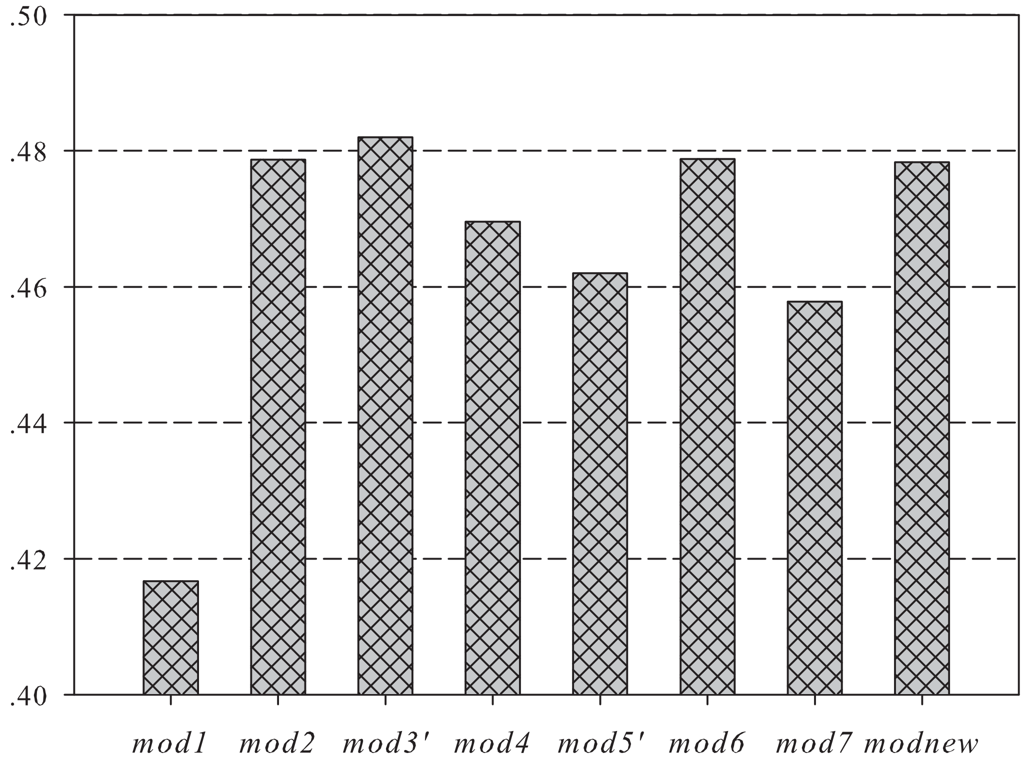

.50
.48
.46
.44
.42
.40
mod1
mod2
mod3'
mod4
mod5'
mod6
mod7
modnew

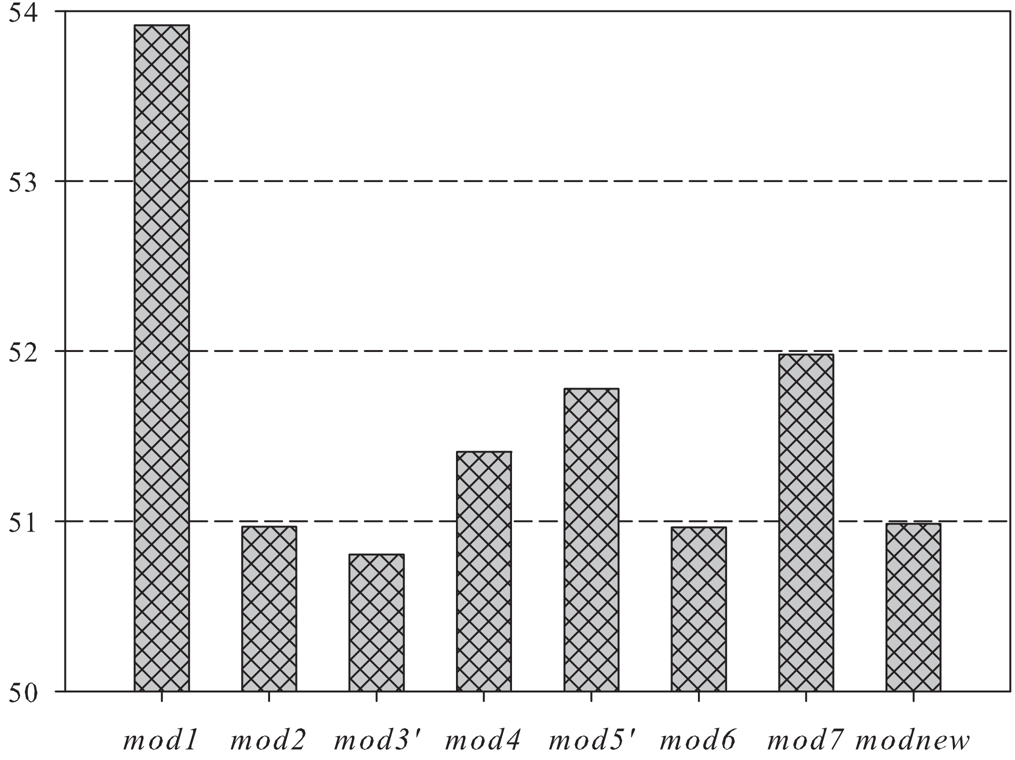

54
53
52
51
50
mod1
mod2
mod3'
mod4
mod5'
mod6
mod7
modnew

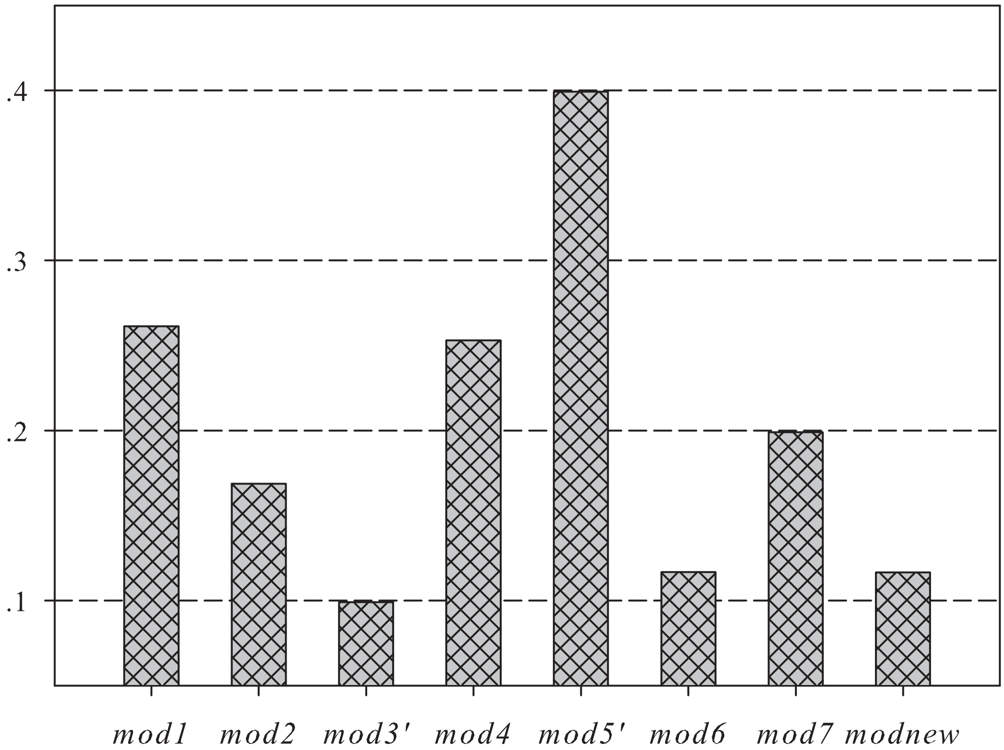

.4
.3
.2
.1
mod1
mod2
mod3'
mod4
mod5'
mod6
mod7
modnew

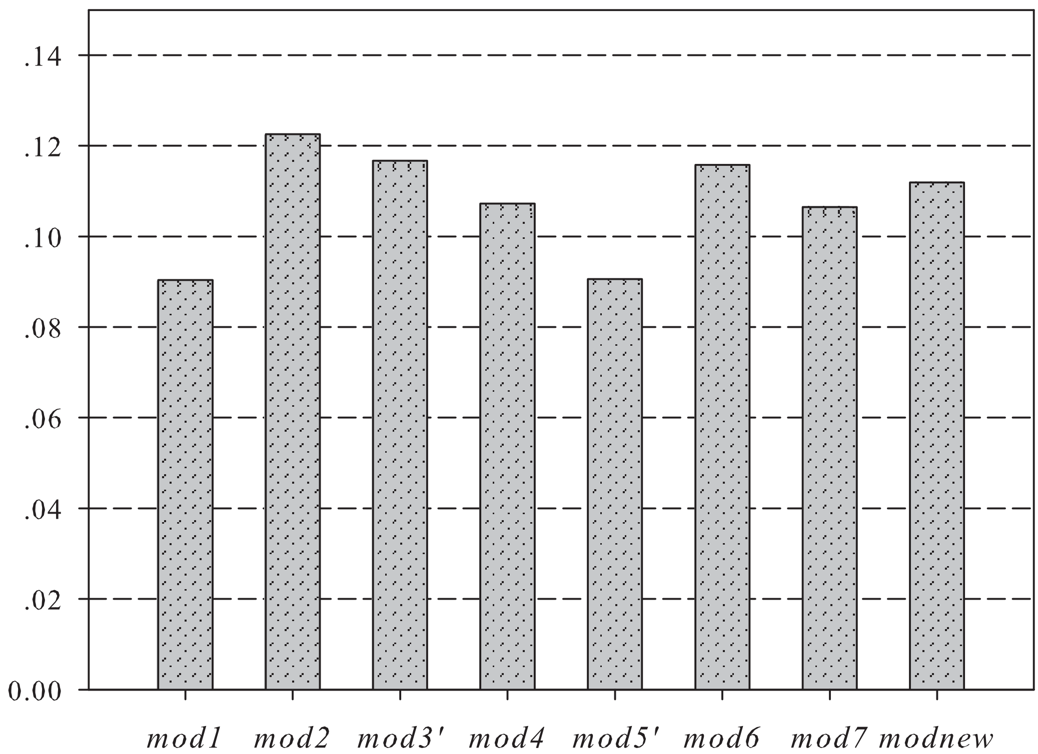
.14
.12
.10
.08
.06
.04
.02
0.00
mod1
mod2
mod3'
mod4
mod5'
mod6
mod7
modnew

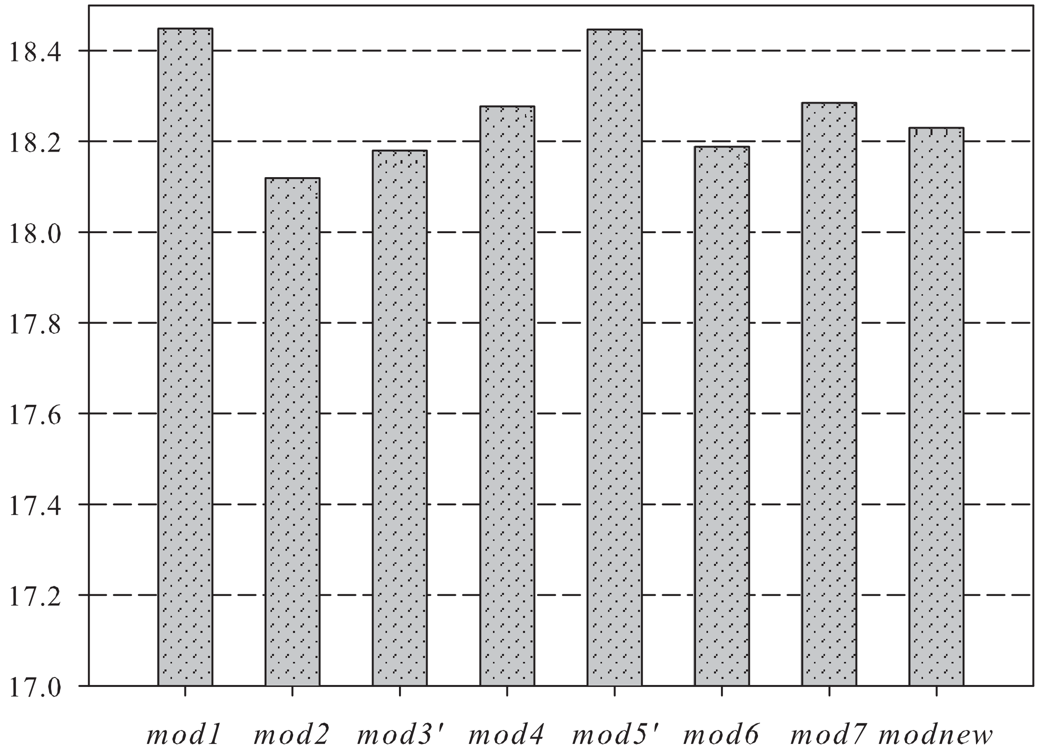

18.4
18.2
18.0
17.8
17.6
17.4
17.2
17.0
mod1
mod2
mod3'
mod4
mod5'
mod6
mod7
modnew

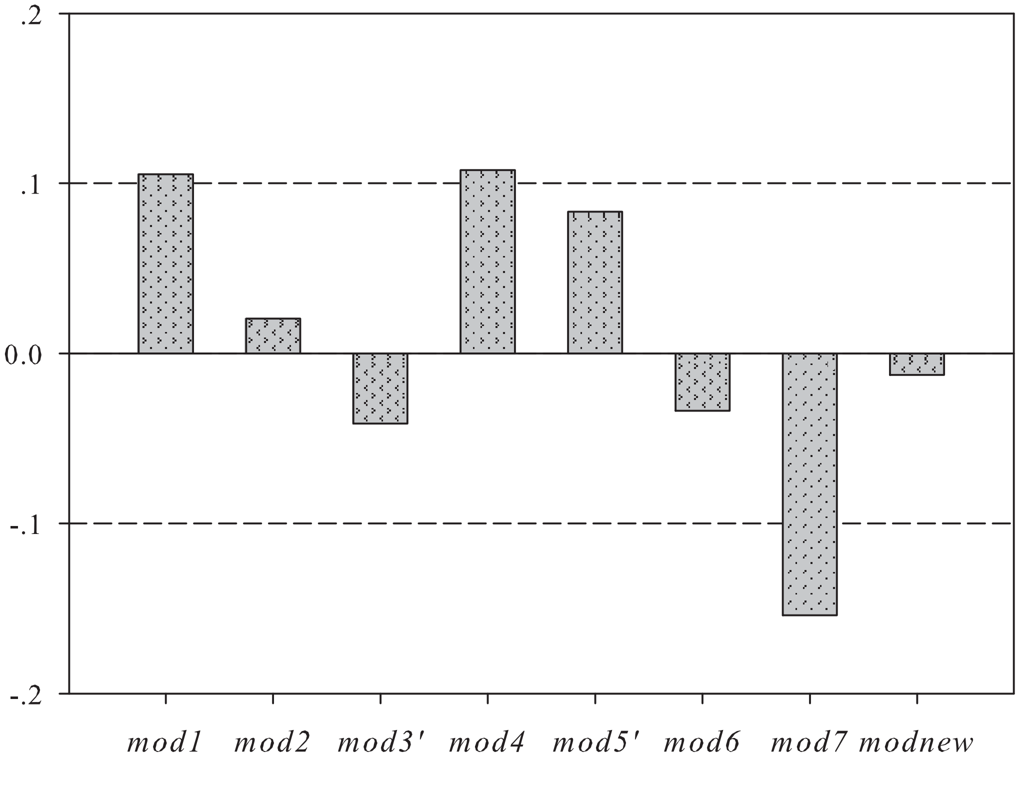
.2
.1
0.0
-.1
-.2
mod1
mod2
mod3'
mod4
mod5'
mod6
mod7
modnew

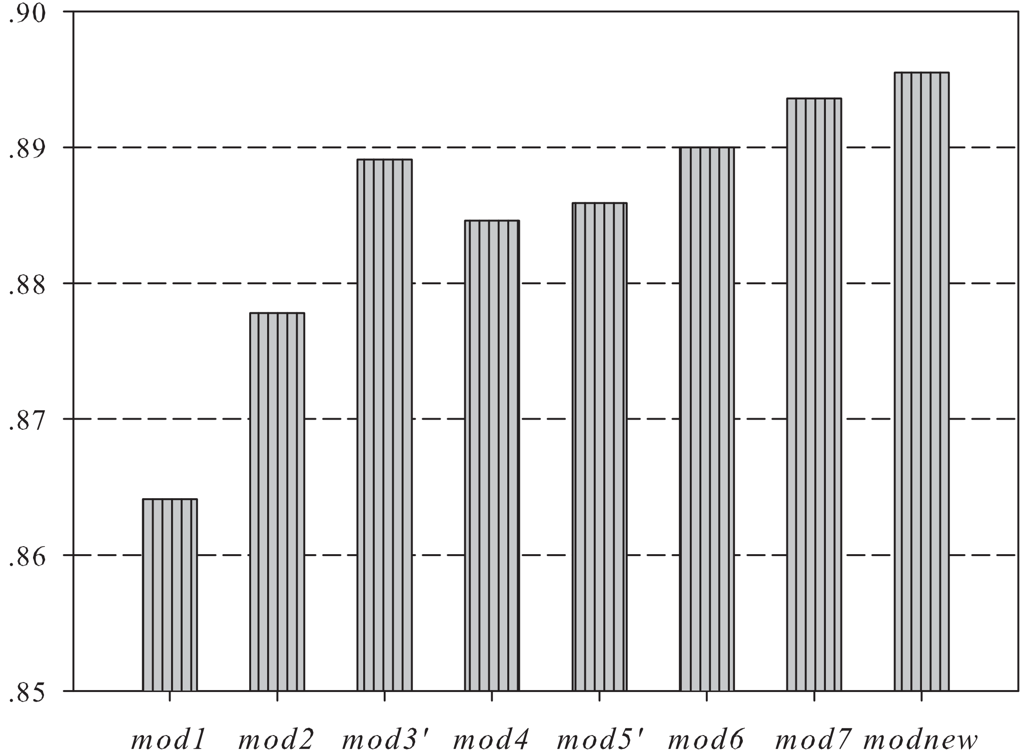

.90
.89
.88
.87
.86
.85
mod1
mod2
mod3'
mod4
mod5'
mod6
mod7
modnew

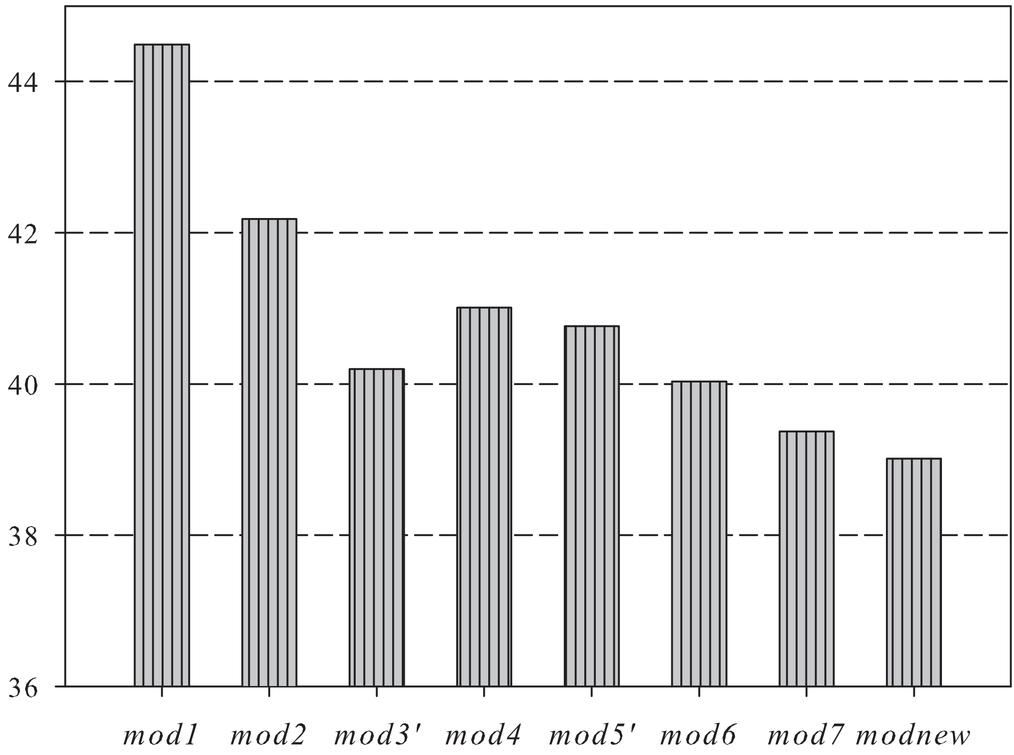
44
42
40
38
36
mod1
mod2
mod3'
mod4
mod5'
mod6
mod7
modnew

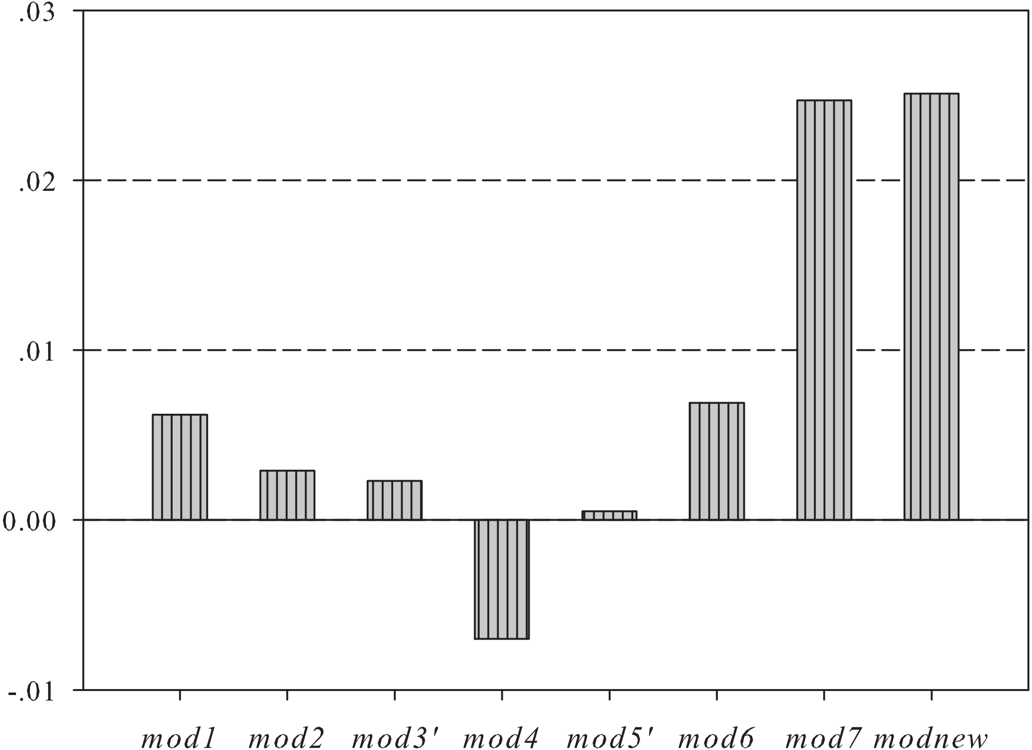

.03
.02
.01
0.00
-.01
mod1
mod2
mod3'
mod4
mod5'
mod6
mod7
modnew

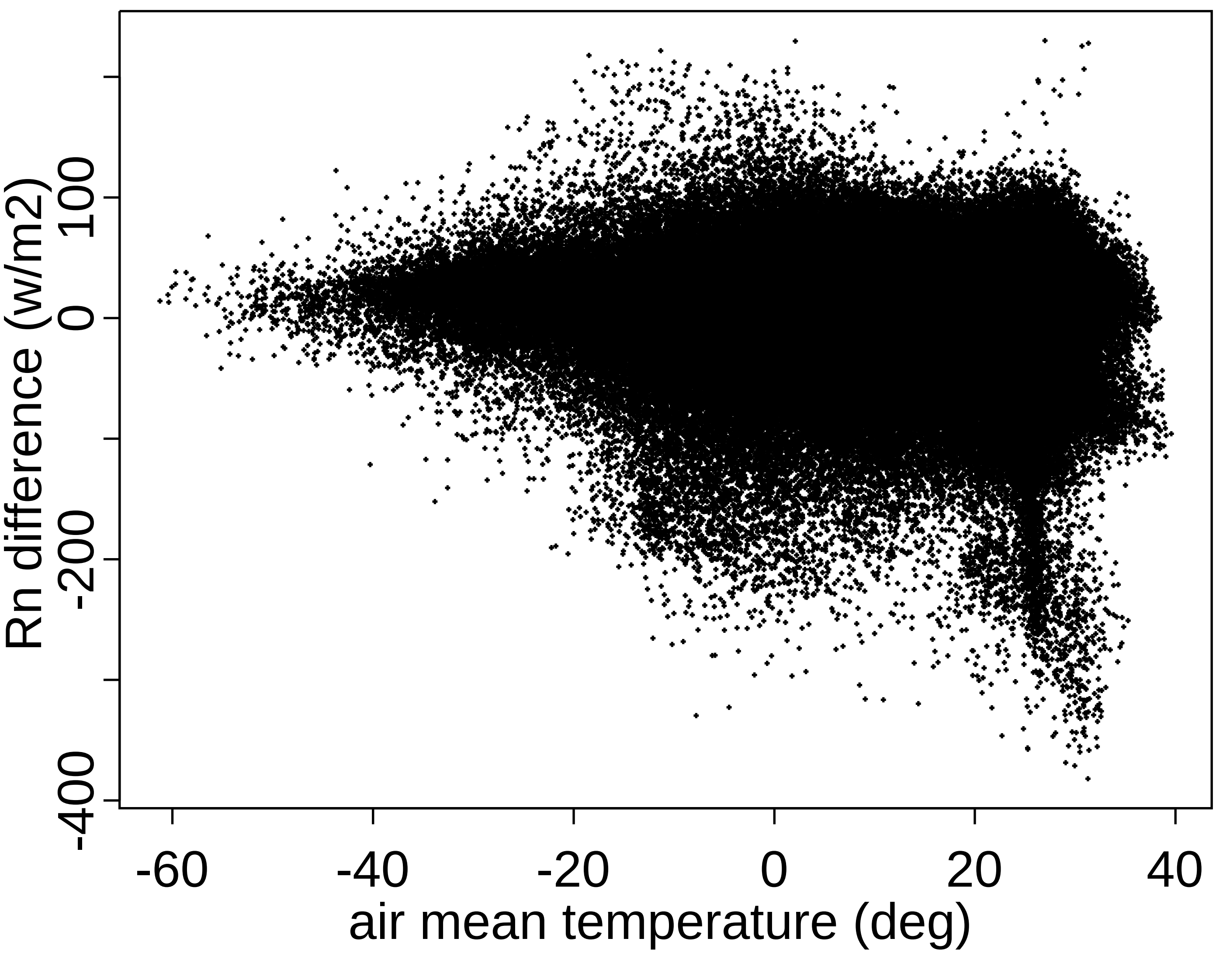

Rn difference (w/m2)
100
0
-200
-400
-60
-40
-20
0
20
40
air mean temperature (deg)

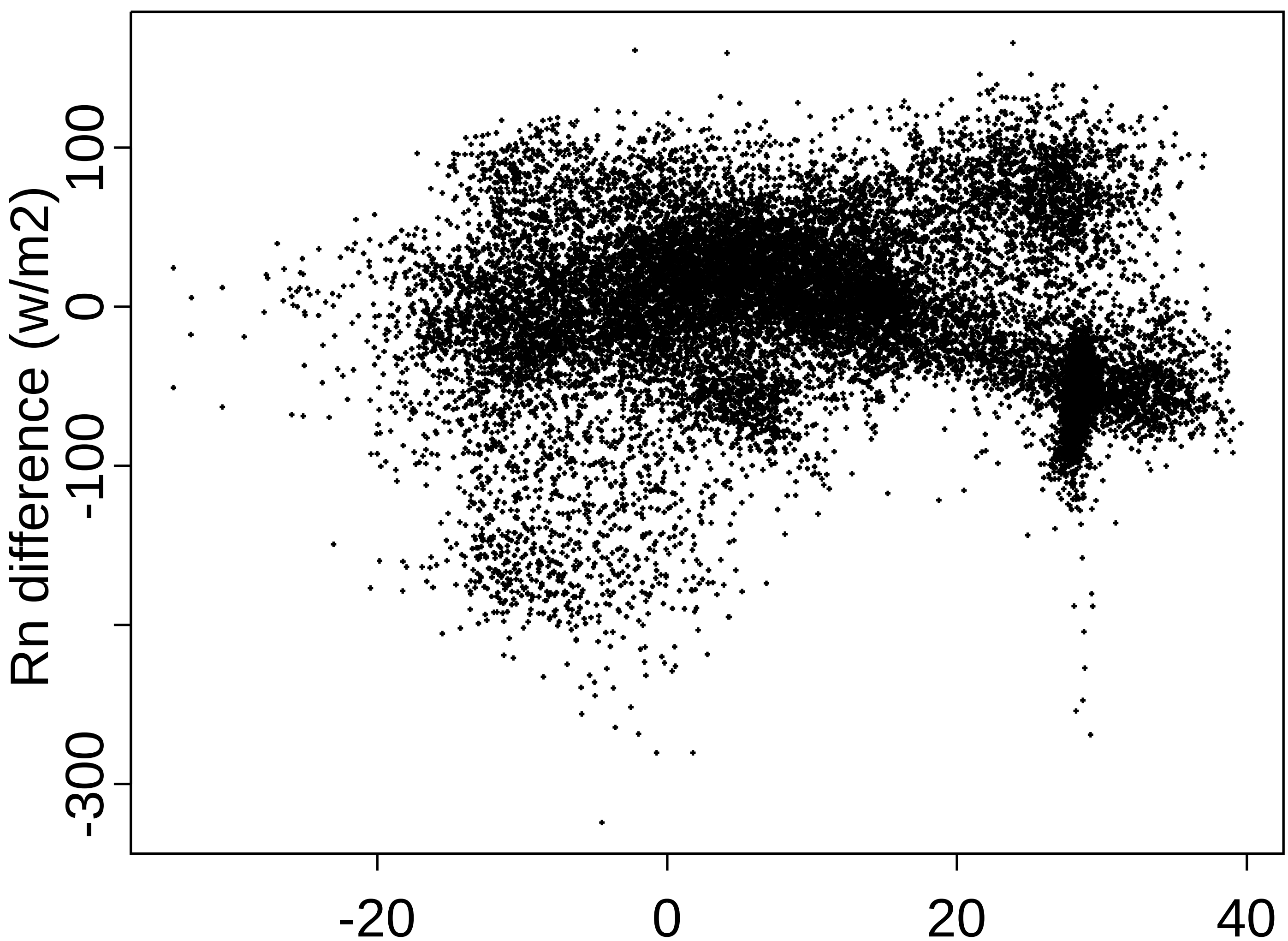

Rn difference (w/m2)
100
0
-100
-300
-20
0
20
40
air mean temperature (deg)

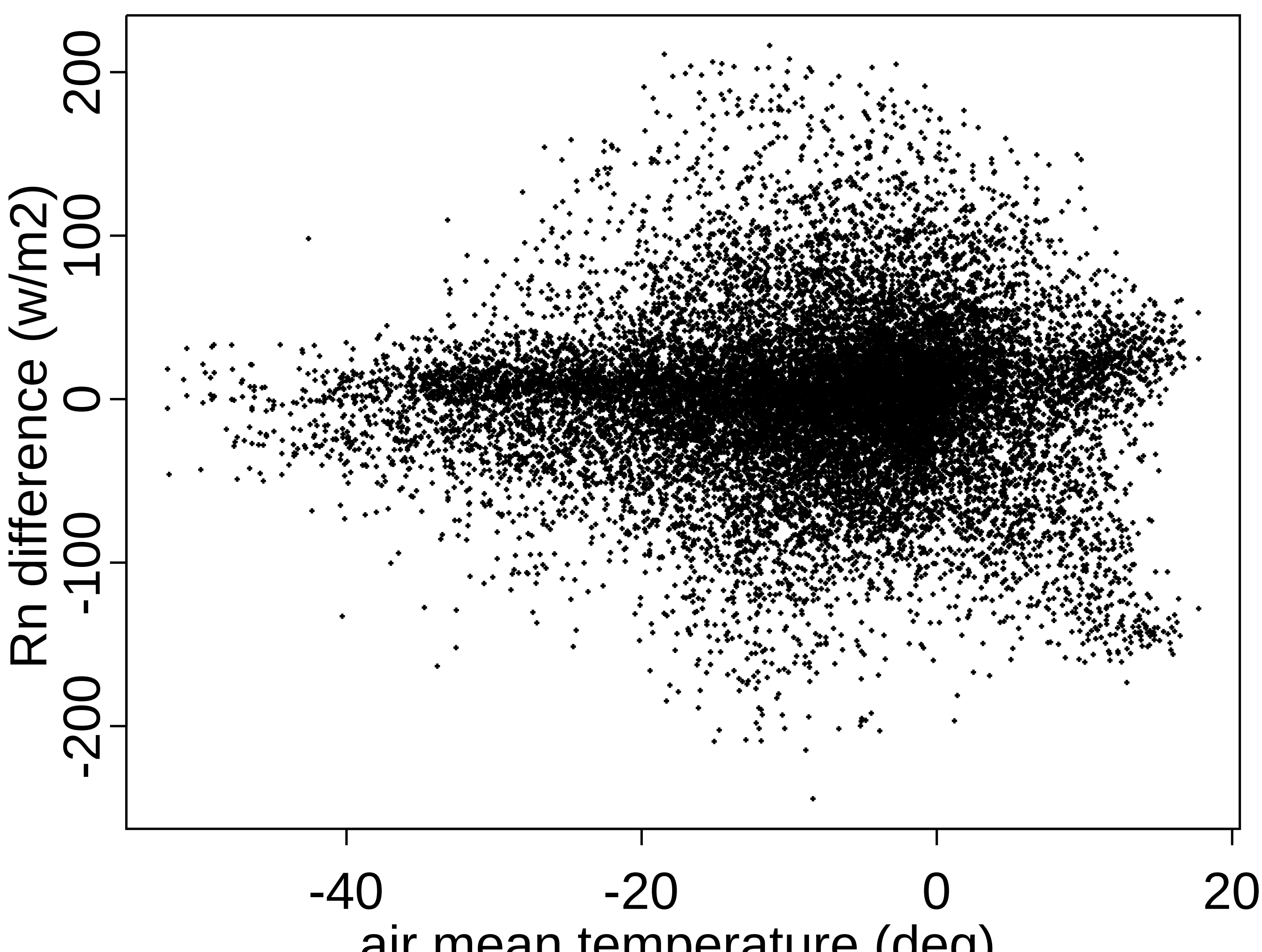
Rn difference (w/m2)
air mean temperature (deg)
200
100
0
-100
-200
-40
-20
0
20

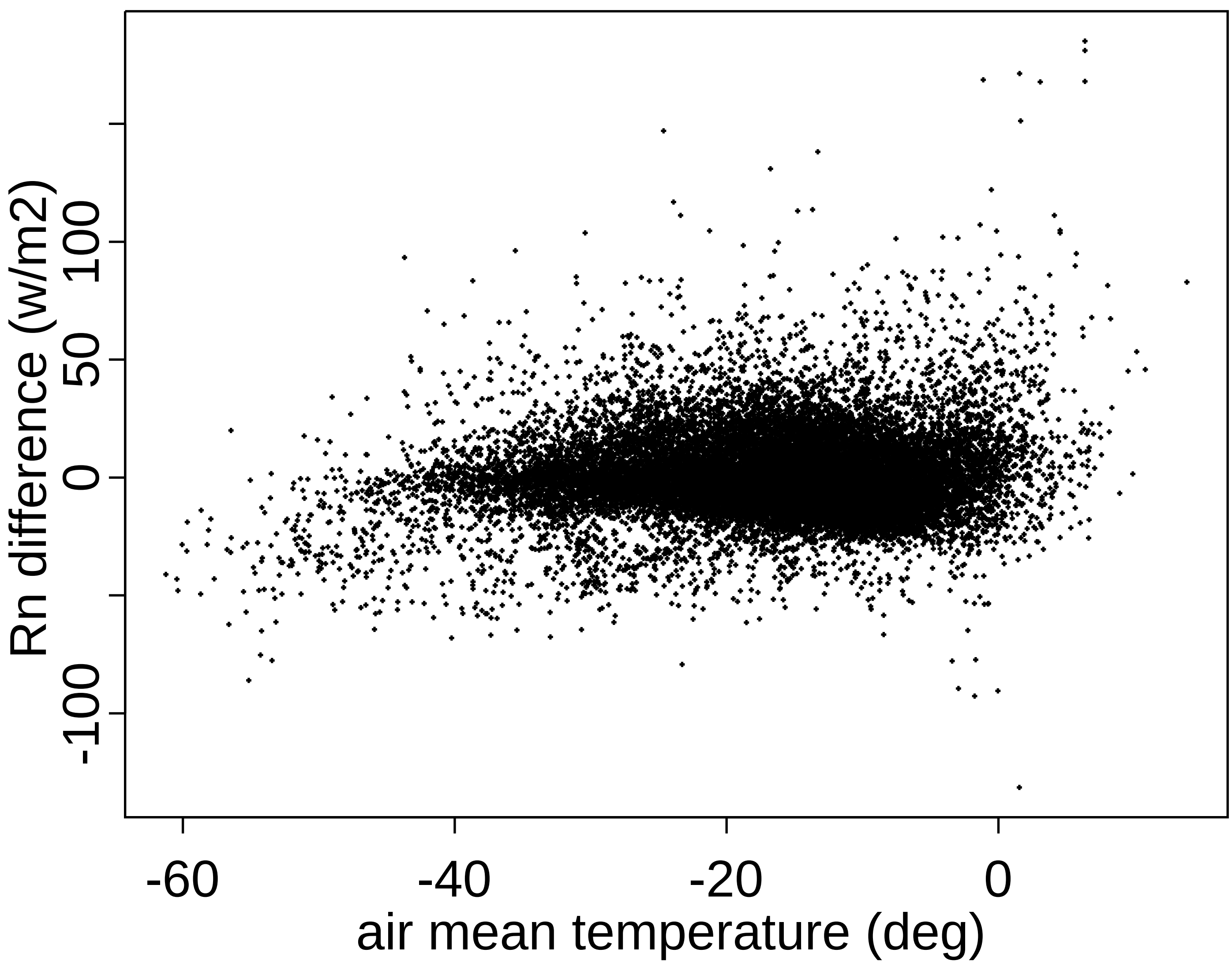
Rn difference (w/m2)
-100
0
50
100
-60
-40
-20
0
air mean temperature (deg)

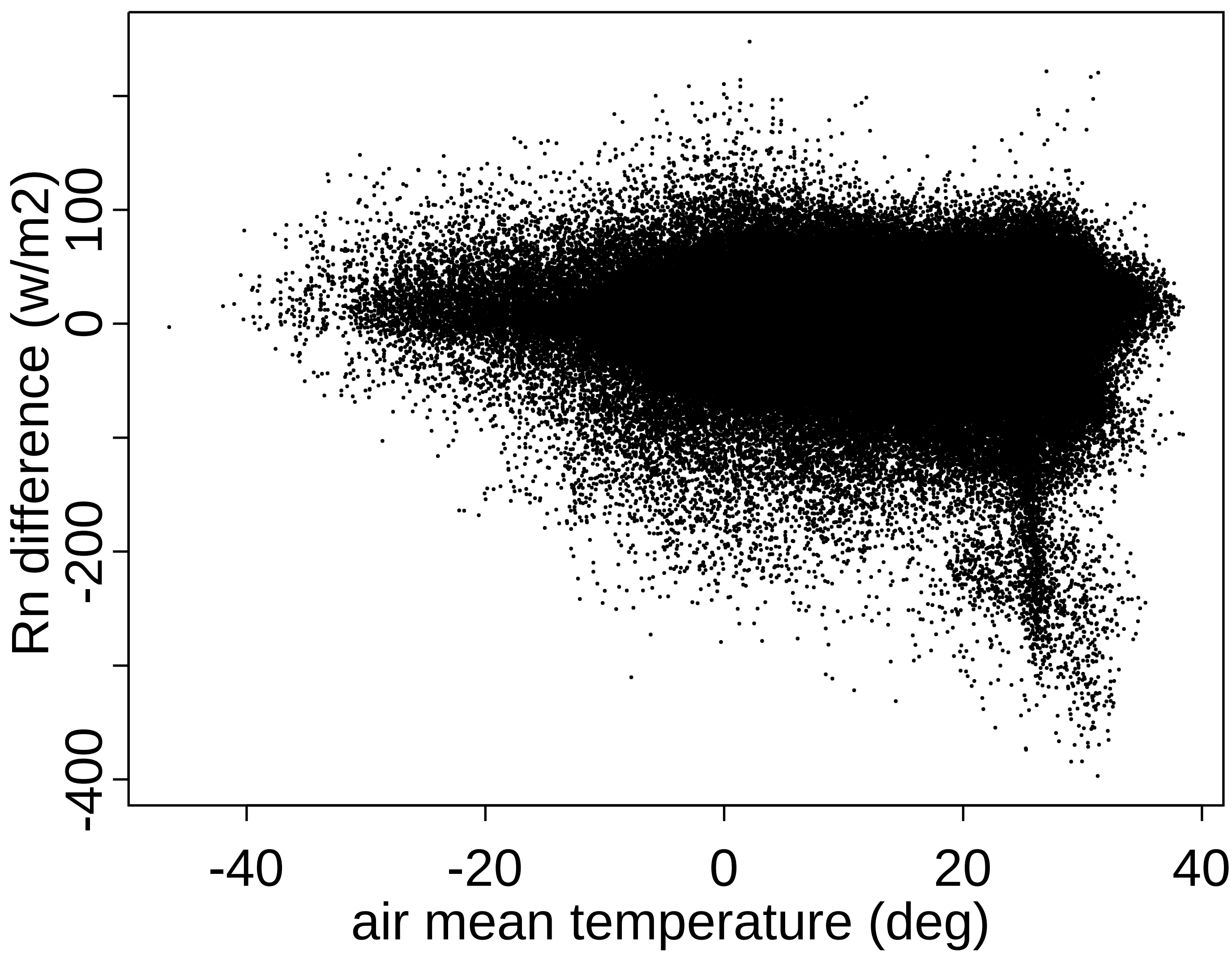

Rn difference (w/m2)
100
0
-200
-400
-40
-20
0
20
40
air mean temperature (deg)

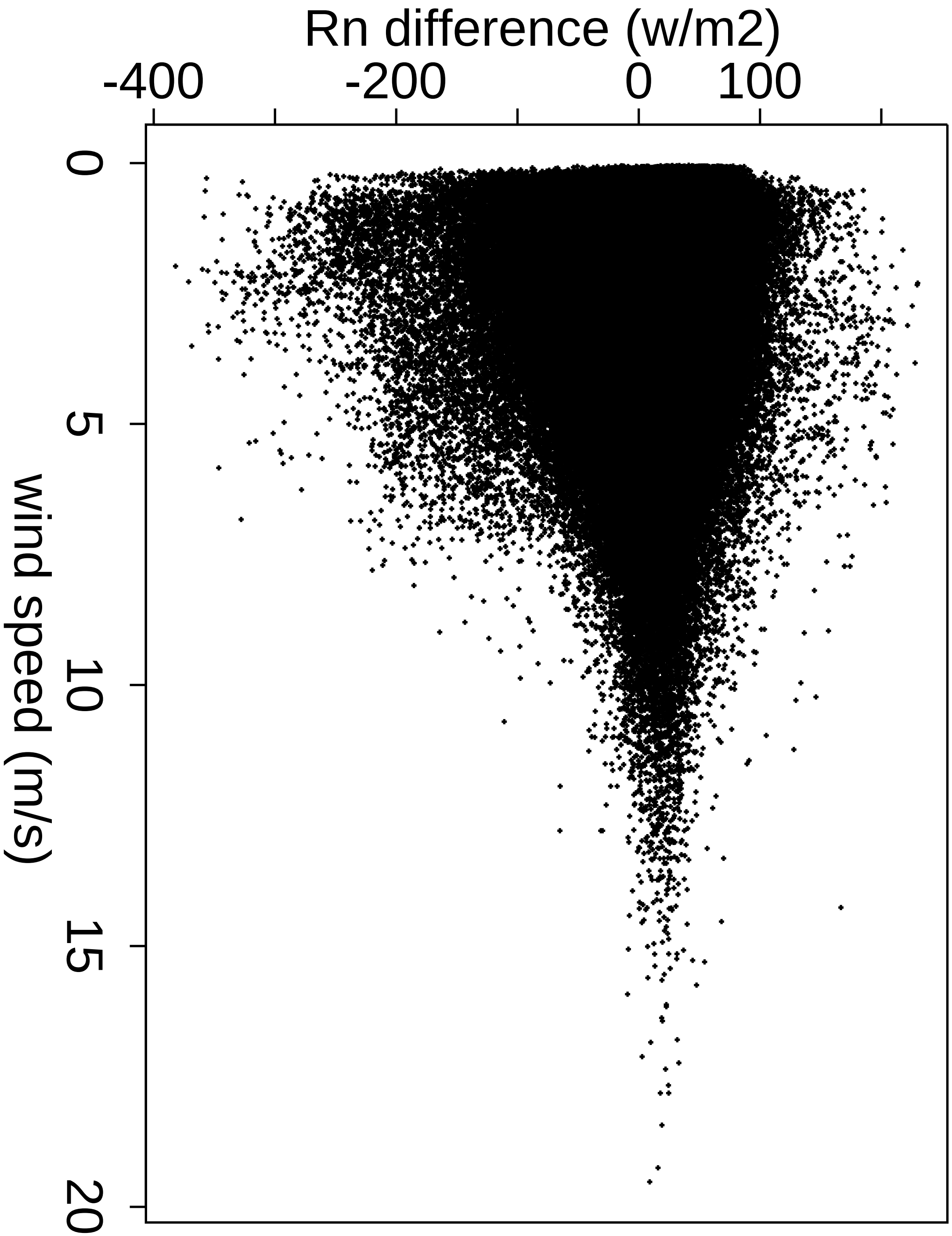
Rn difference (w/m2)
-400
-200
0
100
wind speed (m/s)
0
5
10
15
20

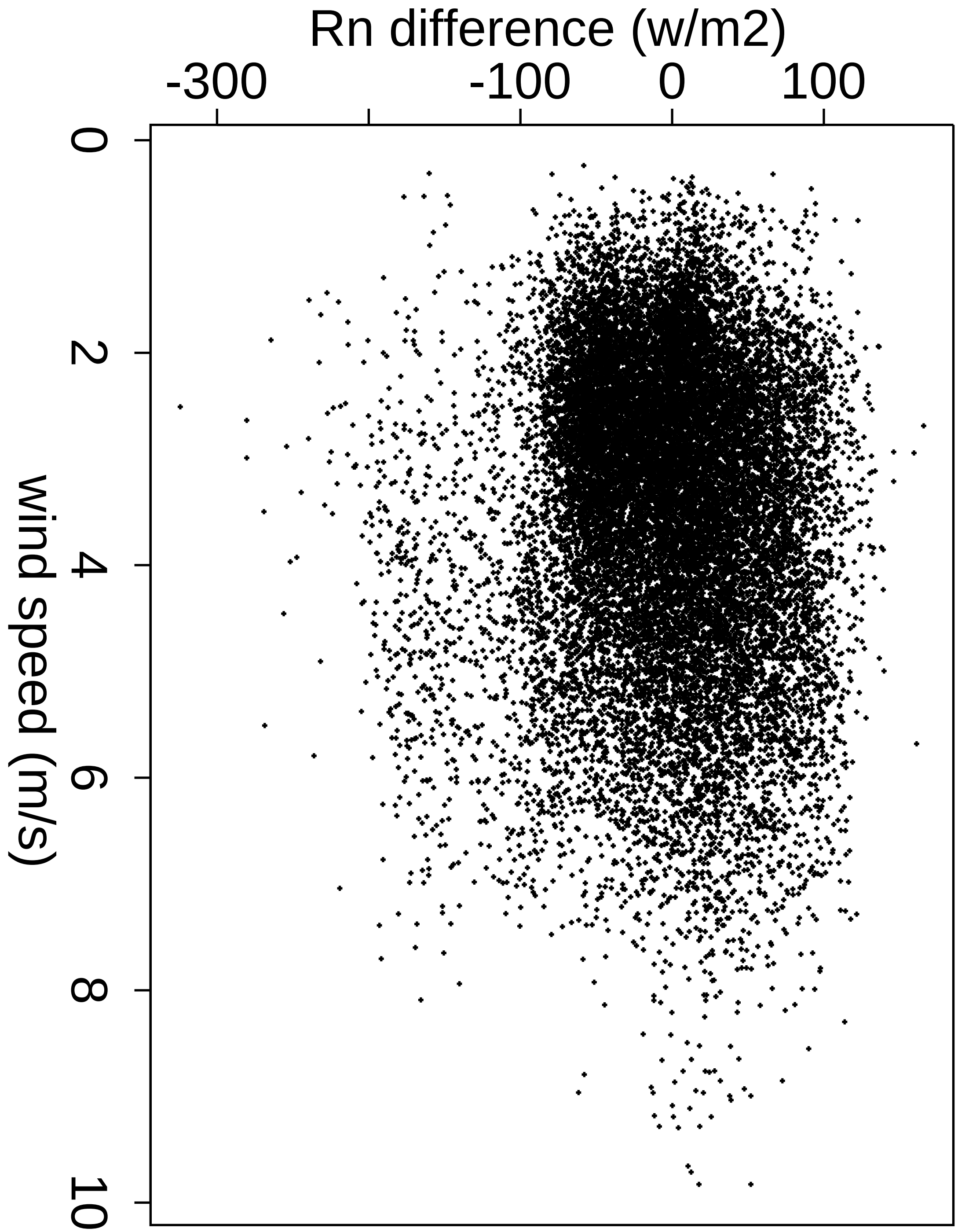

Rn difference (w/m2)
-300
-100
0
100
wind speed (m/s)
0
2
4
6
8
10

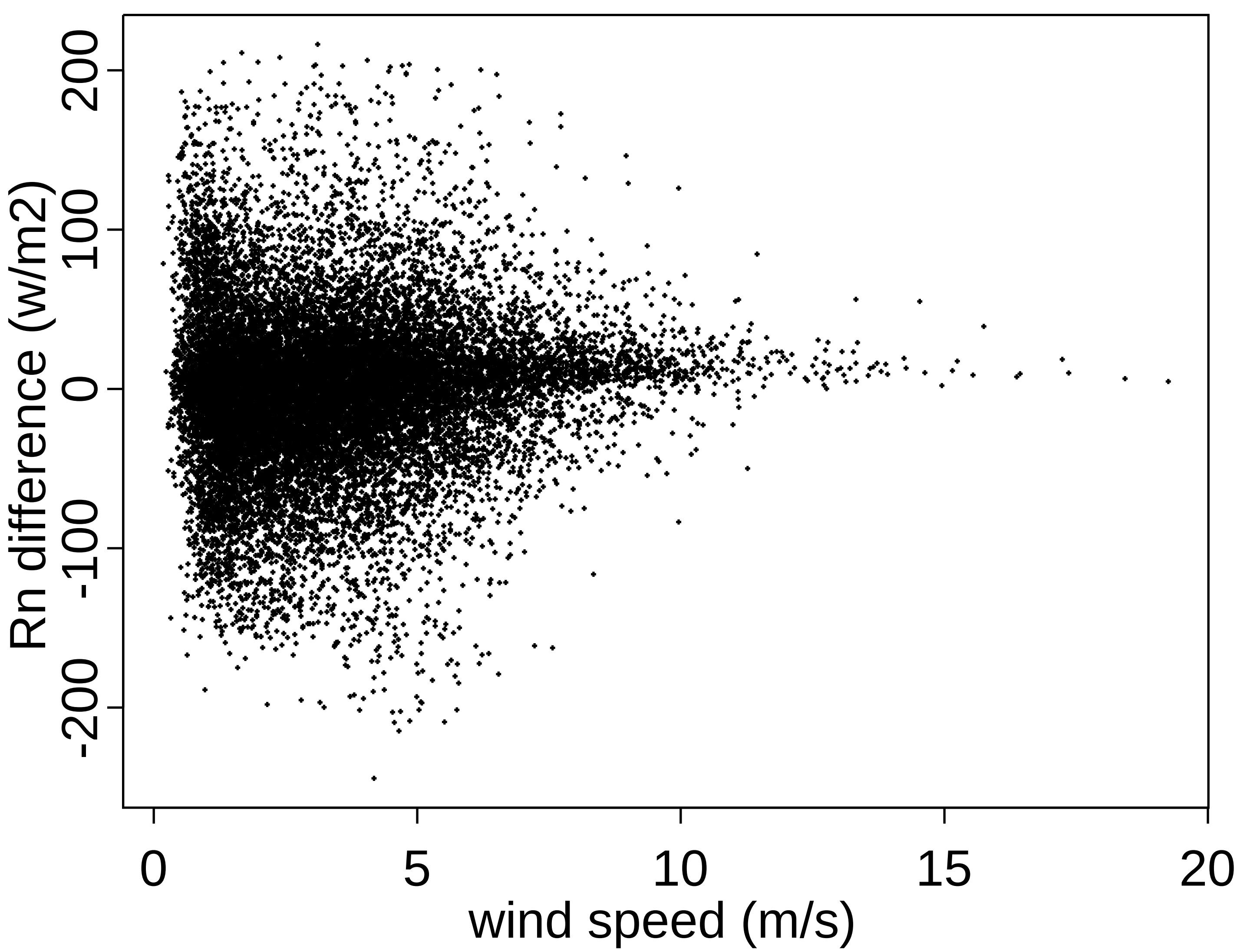

Rn difference (w/m2)
200
100
0
-100
-200
0
5
10
15
20
wind speed (m/s)

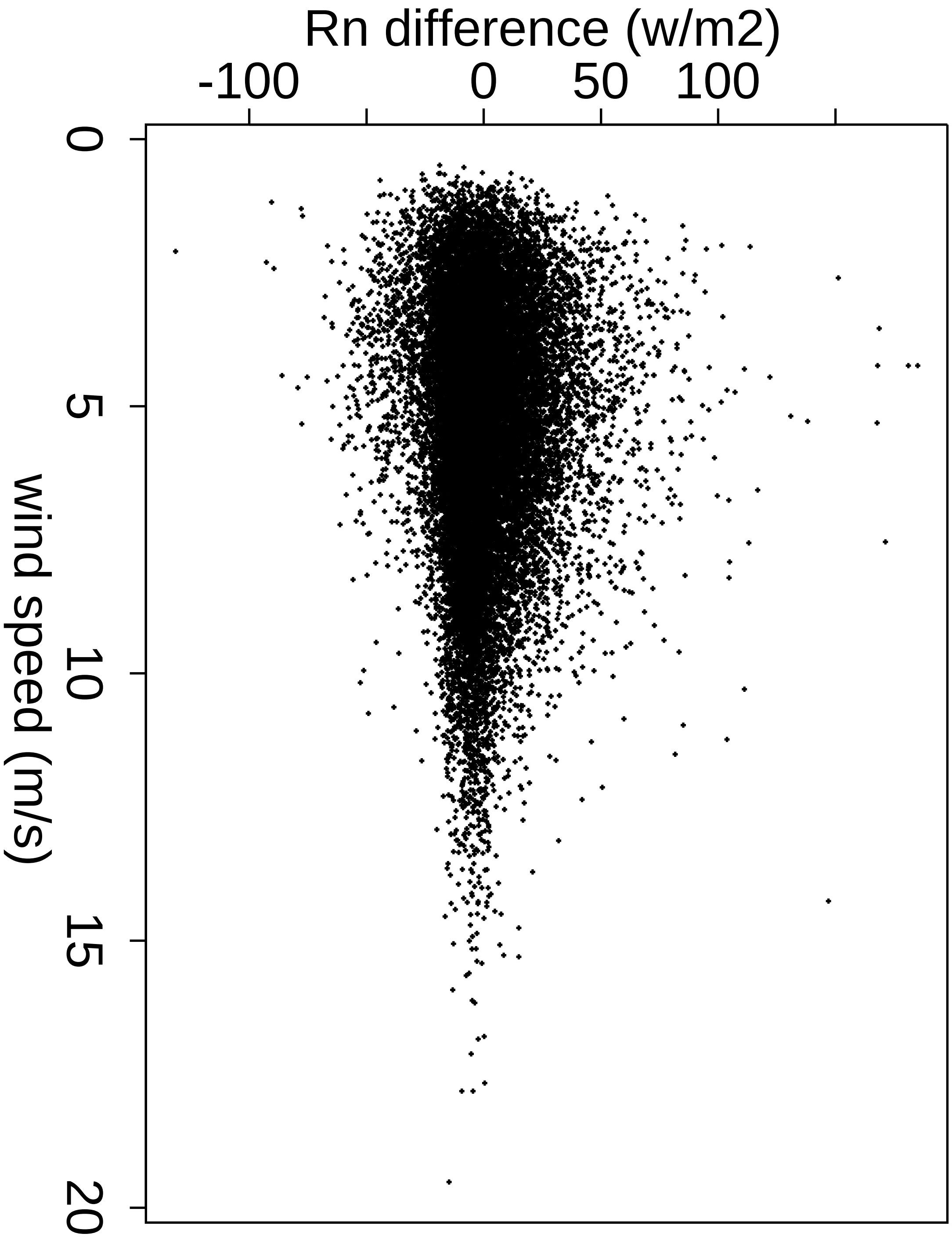

Rn difference (w/m2)
-100
0
50
100
wind speed (m/s)
0
5
10
15
20

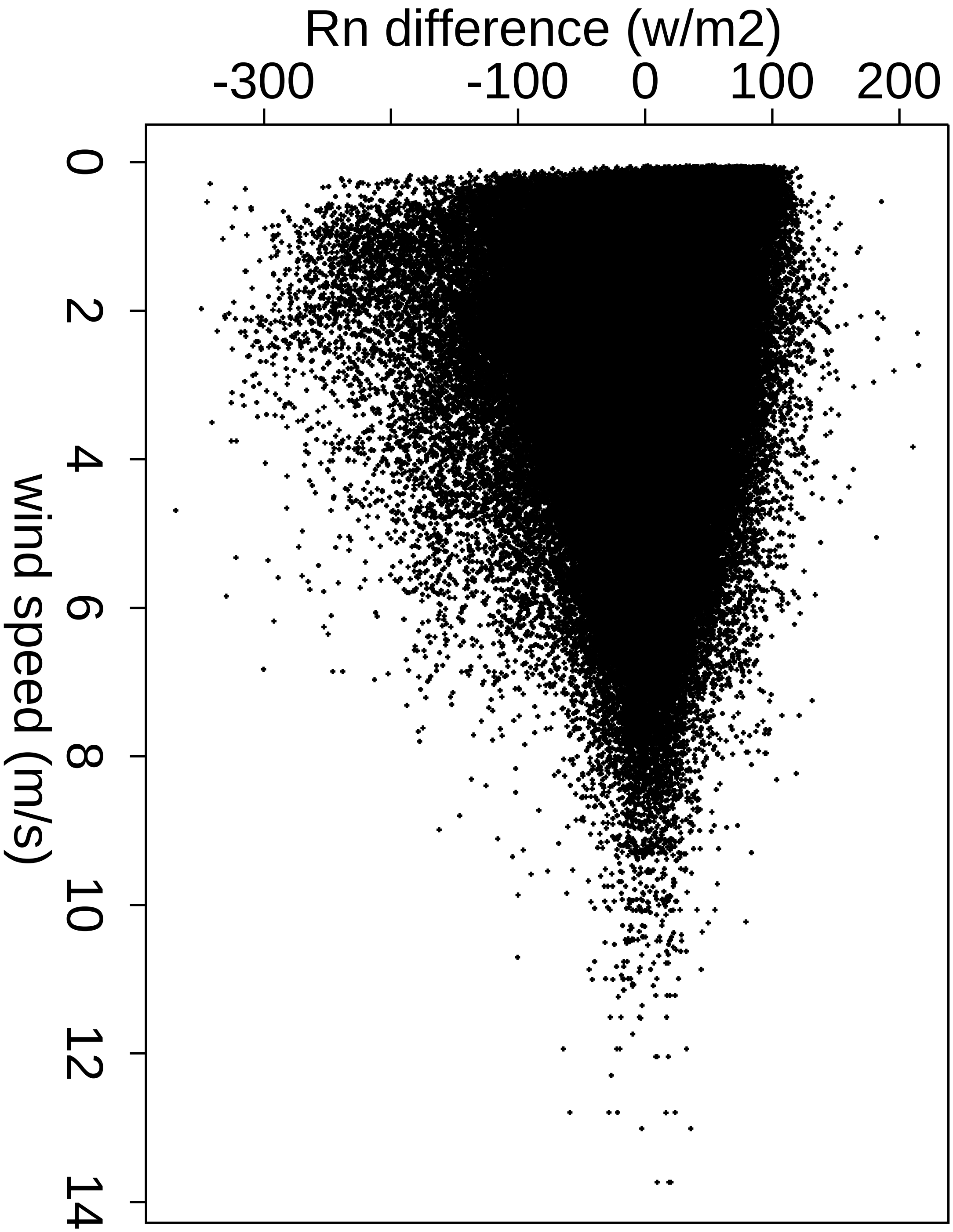
Rn difference (w/m2)
-300
-100
0
100
200
wind speed (m/s)
0
2
4
6
8
10
12
14

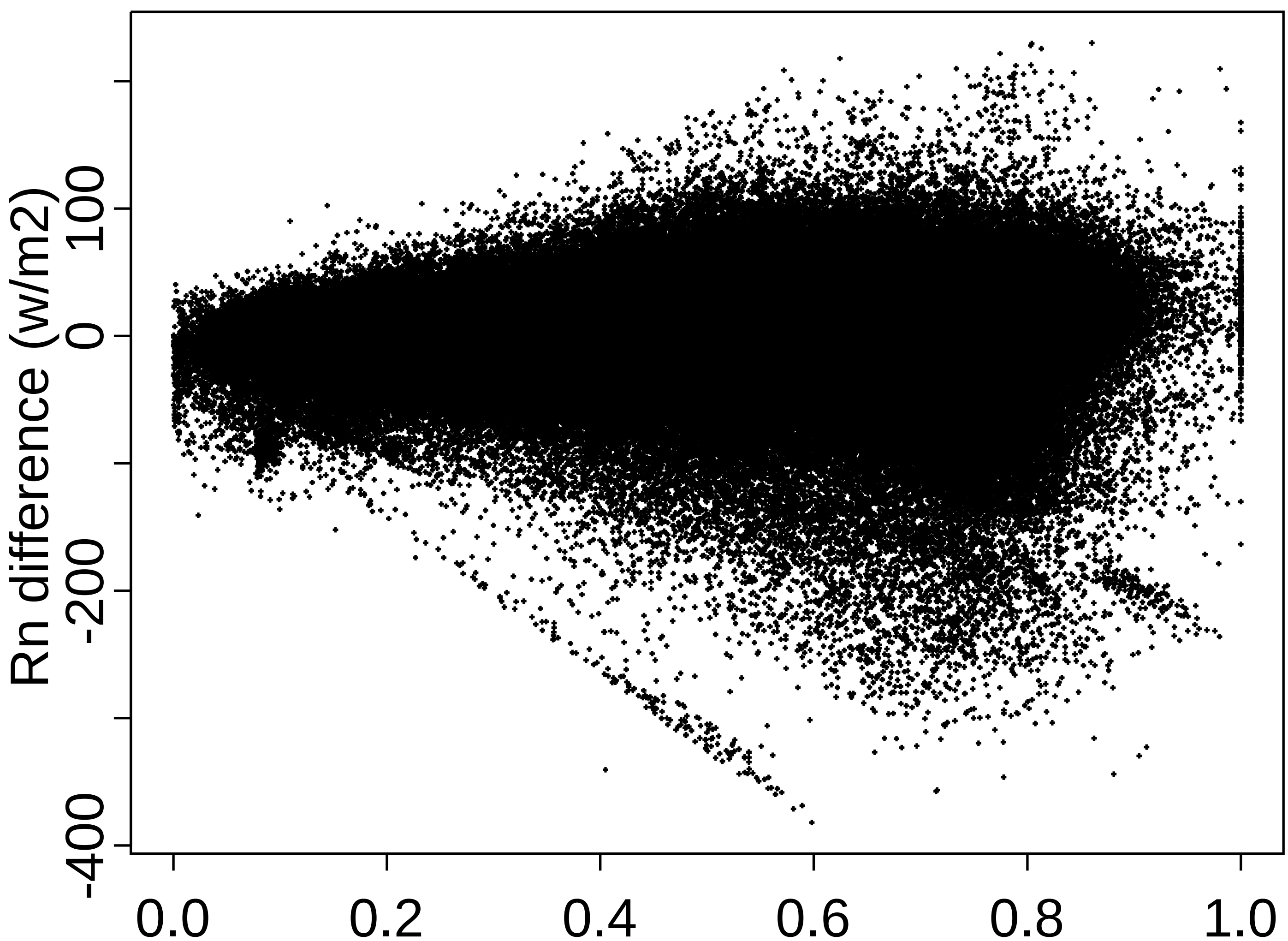

Rn difference (w/m2)
100
0
-200
-400
0.0
0.2
0.4
0.6
0.8
1.0
Clearness Index

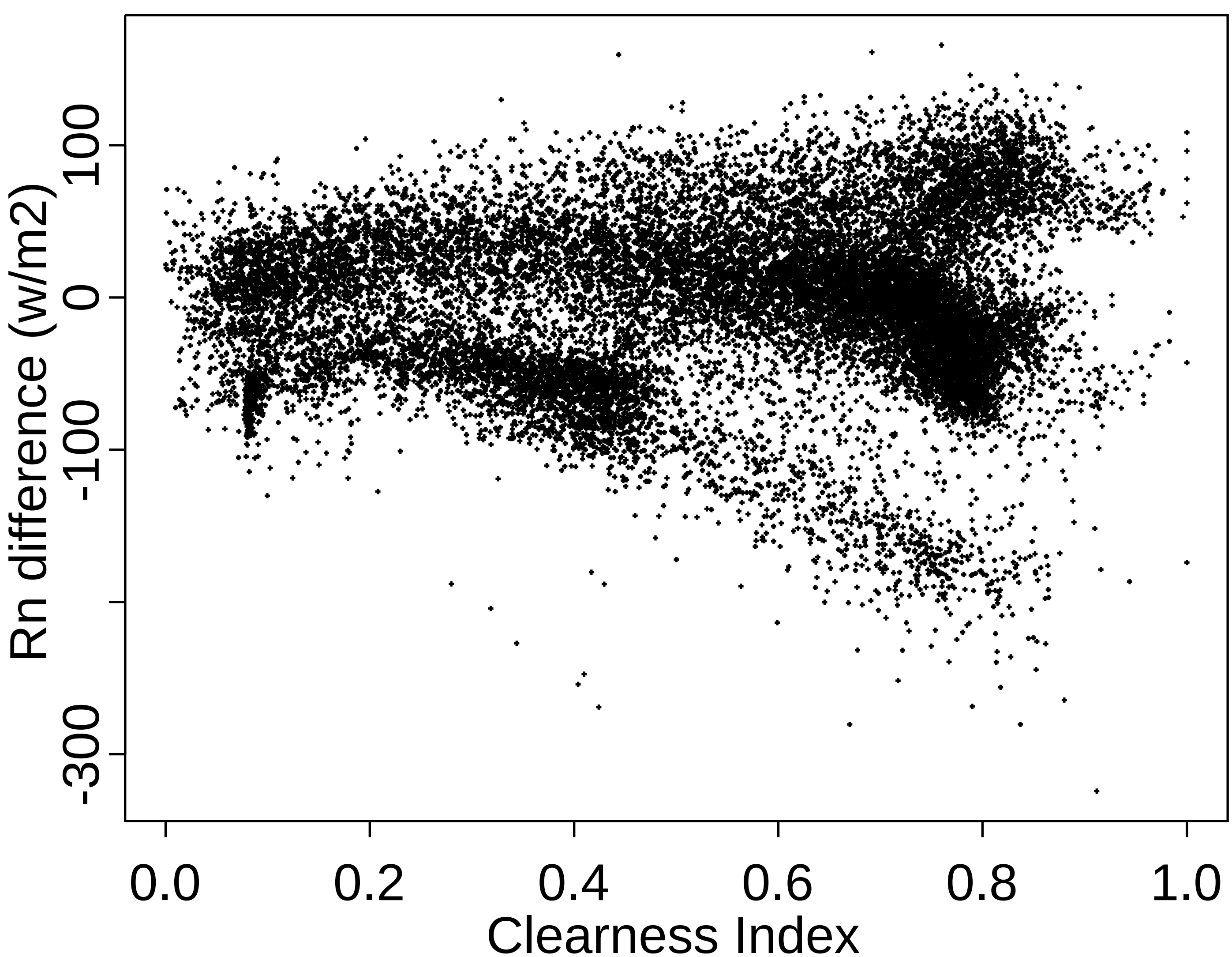

Rn difference (w/m2)
100
0
-100
-300
0.0
0.2
0.4
0.6
0.8
1.0
Clearness Index

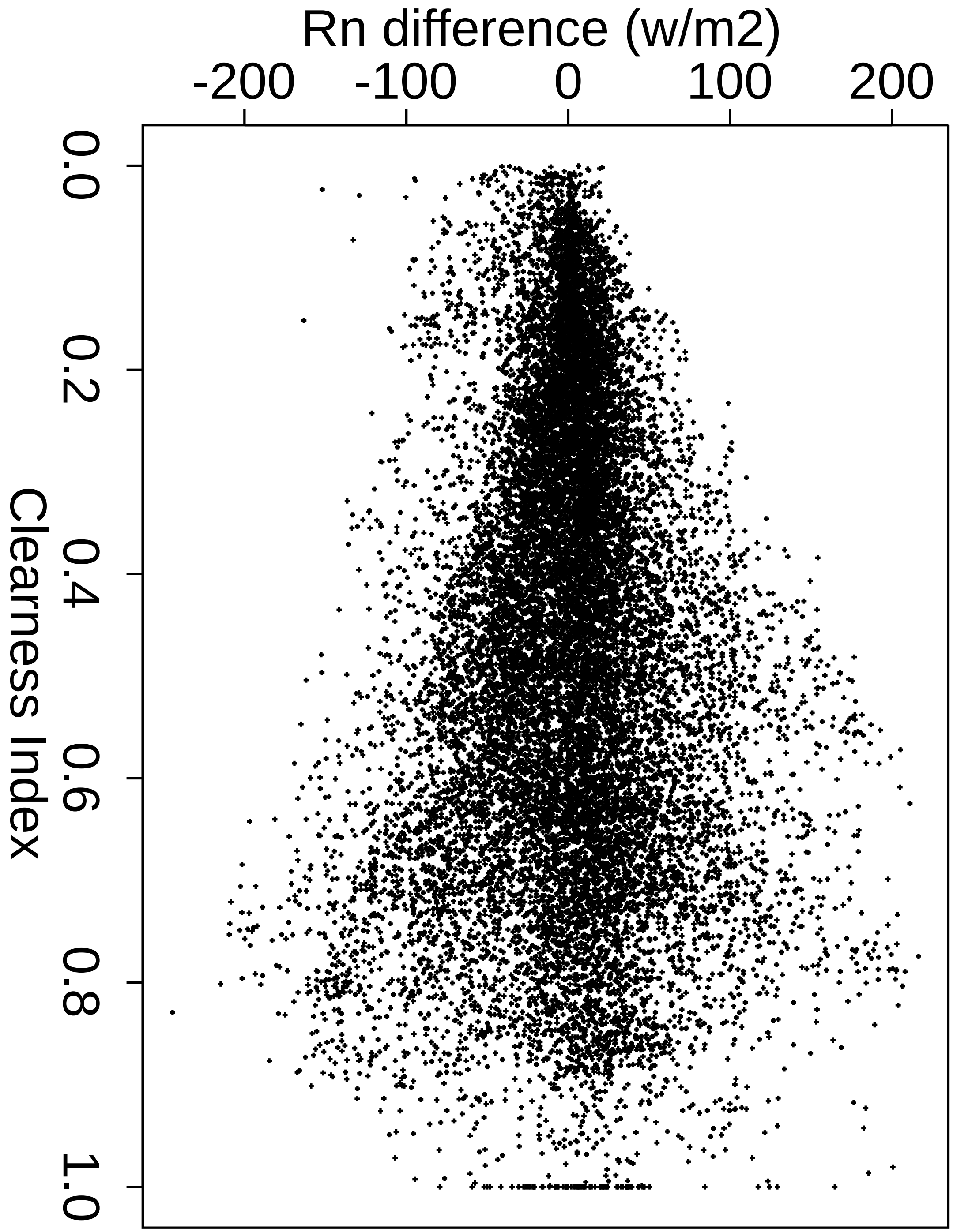
Rn difference (w/m2)
-200
-100
0
100
200
Clearness Index
0.0
0.2
0.4
0.6
0.8
1.0

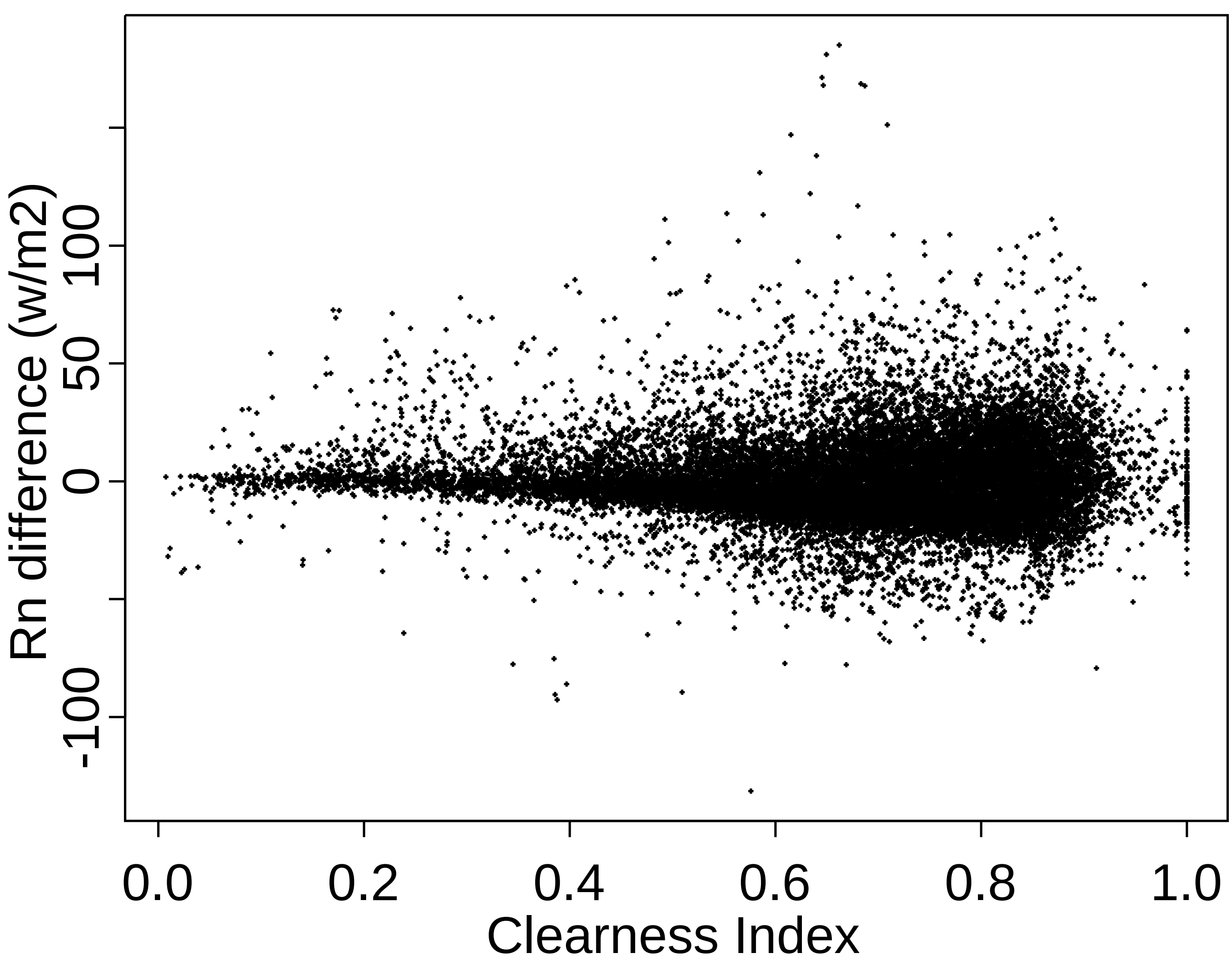

Rn difference (w/m2)
-100
0
50
100
0.0
0.2
0.4
0.6
0.8
1.0
Clearness Index

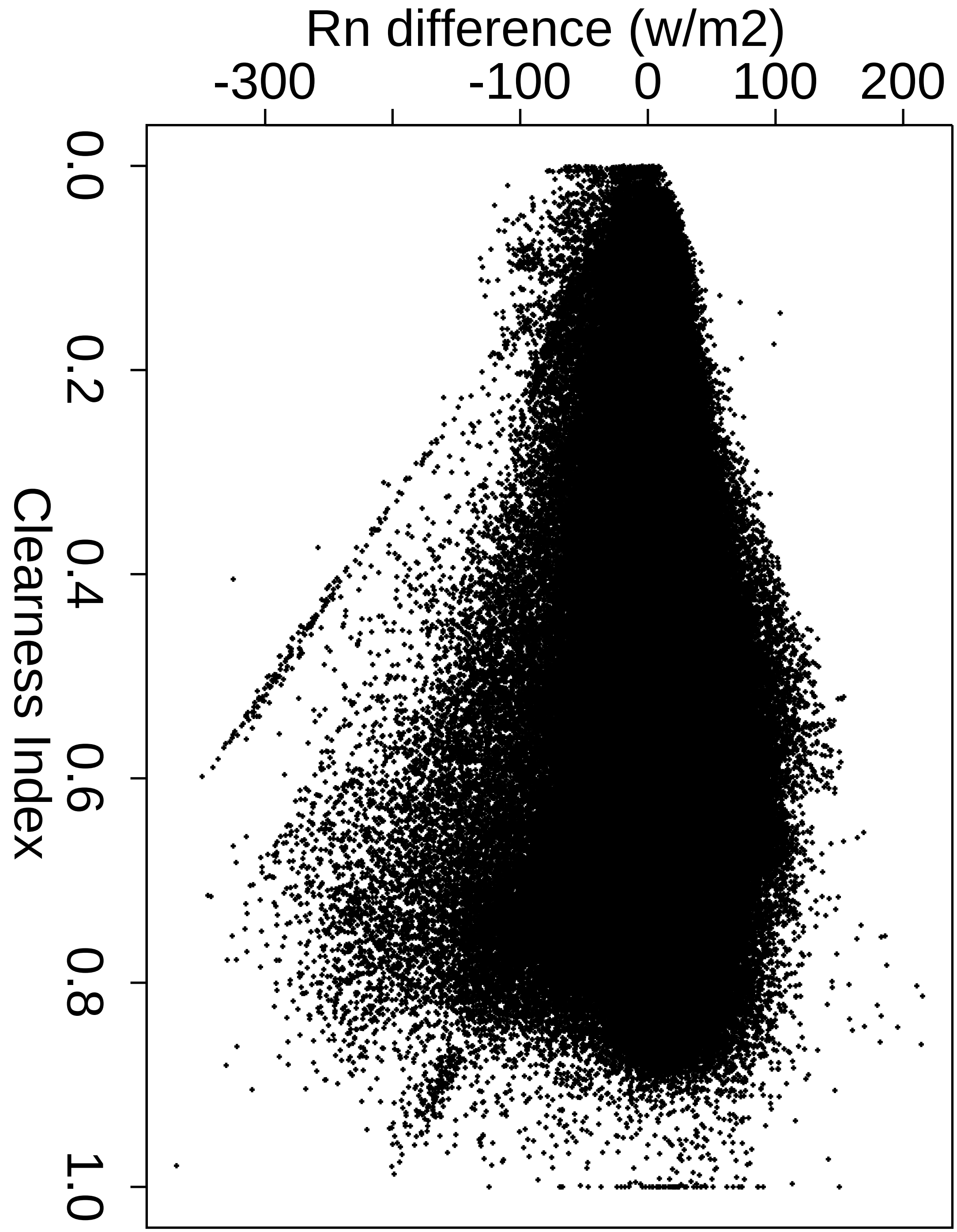
Rn difference (w/m2)
-300
-100
0
100
200
Clearness Index
0.0
0.2
0.4
0.6
0.8
1.0